A table of contents entry

Synergistically complexation of phenol functionalized polymer induced in-situ microfiber formation for 3D printing of marine-based hydrogel

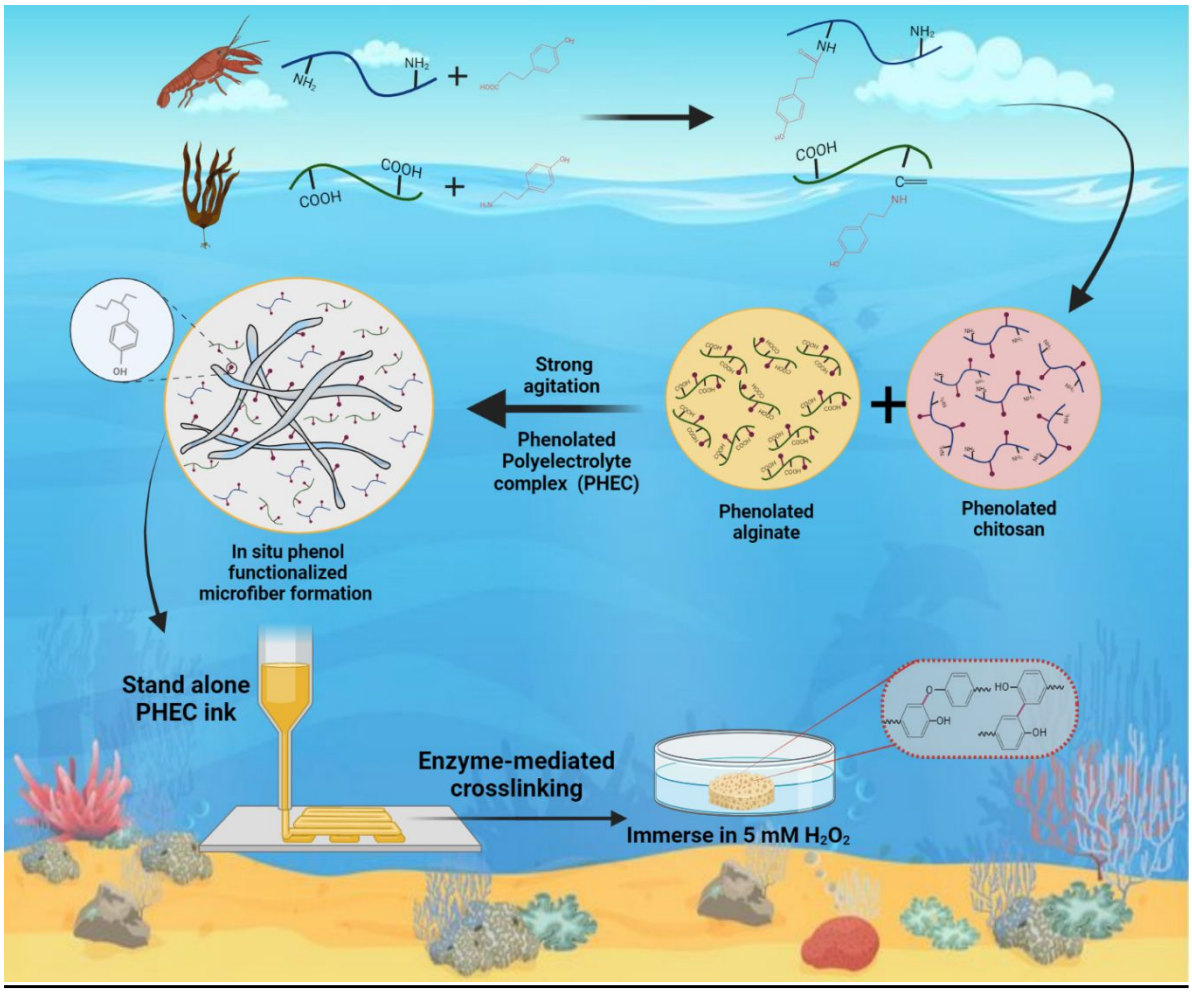

This study proposes a strategy to design tough and 3D printable marine-based hydrogels based on the synergistic complexation of phenolated polyelectrolyte complex and enzyme-mediated crosslinking.

Synergistically complexation of phenol functionalized polymer induced in-situ microfiber formation for 3D printing of marine-based hydrogel

[a]Hafez Jafari*, [b]Christine Delporte, [c]Katrien V. Bernaerts, [d]Houman Alimoradi, [e]Lei Nie, [f]Daria Podstawczyk, [g]Kam Chiu Tam*, [a]Amin Shavandi*

[a] Université libre de Bruxelles (ULB), École polytechnique de Bruxelles - BioMatter unit, Avenue F.D. Roosevelt, 50 - CP 165/61, 1050 Brussels, Belgium.

[b]Laboratory of Pathophysiological and Nutritional Biochemistry, Faculty of Medicine, Université libre de Bruxelles (ULB), Route de Lennik, 808 – CP611, 1070 Brussels, Belgium

[c]Maastricht University, Aachen-Maastricht Institute for Biobased Materials (AMIBM), Brightlands Chemelot campus, Urmonderbaan 22, 6167 RD Geleen, the Netherlands

[d] School of Biomedical Sciences, University of Otago, Dunedin, New Zealand

[e] College of Life Sciences, Xinyang Normal University (XYNU), Xinyang 464000, China.

[f] Department of Process Engineering and Technology of Polymer and Carbon Materials, Faculty of Chemistry, Wroclaw University of Science and Technology, Norwida 4/6, Wroclaw, 50-373 Poland;

[g] Department of Chemical Engineering, Waterloo Institute for Nanotechnology, University of Waterloo, 200 University Avenue West, Waterloo, Ontario N2L 3G1, Canada

* Corresponding authors: Email: Hafez.Jafari@ulb.be, mkctam@uwaterloo.ca, amin.shavandi@ulb.be, Tel: +326503681(A.S)

Abstract

The design of 3D printable bio-based hydrogels with enhanced mechanical properties and minimal chemical modification can open new opportunities in the field of biomedical applications. A facile and safe approach is proposed to prepare mechanically reinforced chitosan-based hydrogels via a phenolated polyelectrolyte complex (PHEC) and enzyme-mediated crosslinking. PHEC was formed between phenolated chitosan and alginate, leading to the formation of *in situ* phenol-functionalized microfibers that exhibited excellent 3D printability. The synergistic complexation enhanced the loss modulus (60 times), toughness (2-3 times), flexibility, moldability, and dynamic viscosity (20 times) of the hydrogel compared to individual phenolated chitosan and alginate hydrogels. This complexation endowed the material with excellent printability without sacrificing the hydrogel's elasticity. This study proposes a strategy to design tough and 3D printable marine-based hydrogels based on the synergistic complexation of phenolated polyelectrolyte complex and enzyme-mediated crosslinking.

Keywords: Phenolated polyelectrolyte complex; enzyme-mediated crosslinking; *in situ* microfibers

Introduction

In recent years, there has been an increasing interest in developing bioprintable hydrogels for tissue engineering and wound healing applications[1]. However, biopolymer-based hydrogels generally lack the required resilience and toughness for biomedical applications, such as tissue regeneration, wound healing, and wearable sensors [2]. The toughness and viscoelasticity of hydrogels can be improved by incorporating high aspect ratio fillers such as microfibres and nanowhiskers [3]. Another way of improving the mechanical properties of biobased hydrogels is combining additional covalent or physical interactions or synthetic polymers to form a tough and flexible hydrogel by increasing the energy dissipation of hydrogels [4, 5]. Among the biopolymers, polysaccharides such as chitin, chitosan, alginate, hyaluronic acid, and dextran have been widely used to develop bio-based hydrogels due to their biocompatibility and biodegradability [6].

However, natural polysaccharides have poor mechanical strength, low elasticity, easy breakability, and brittleness which hamper the biomedical application of natural hydrogels. Chitosan is extensively used

in hydrogel development for biomaterials engineering with inherent biological properties such as antioxidant, antibacterial, and anti-inflammatory activity [7-9]. However, in addition to low solubility, the poly-β-(1,4)-D-glucosamine structure endows the chitosan hydrogel with high rigidity and an unsatisfactory energy dissipation mechanism resulting in brittle hydrogels [10-12].

The introduction of reversible interactions as secondary crosslinks to chitosan hydrogels can resolve the limitation caused by the polysaccharides' rigidity. For example, Xu et al. developed a series of chitosan/vanillin hydrogels originating from reversible Schiff base reactions between the aldehyde group of vanillin and the amino group of chitosan [13]. However, Schiff-base linkage can be hydrolyzed under acidic conditions, which hampers its applicability [14]. Besides, Zhou et al. developed a tough and self-healable chitosan/polyacrylic acid hydrogel via the conjugation of quaternary ammonium groups onto the chitosan backbone [15]. However, the time-consuming grafting process of the quaternized amino groups with extensive use of chemicals such as sodium bicarbonate, sodium borohydride, and methanol as well as the low biocompatibility of polyacrylic acid, hindered the biomedical application of the hydrogel [10].

Furthermore, several methods have reported on the 3D printability of chitosan-based hydrogels. Wu et al. reported a solvent evaporation method for 3D printing of chitosan pre-solution in acidic media [16]. Zhou et al. printed chitosan pre-solution (alkali solution) using a high-temperature method [17]. However, long fabrication time and the use of acidic or alkali media to dissolve the chitosan pre-gel solution in these methods render it unsuitable for direct cell encapsulation and biomedical application. Alternatively, Liu et al. reported a 3D printed chitosan-based hydrogel using photocrosslinking of phenol functionalized chitosan and dibenzaldehyde-terminated telechelic poly(ethylene glycol) (DF-PEG) pre-gel crosslinked by dynamic imine bonds [18]. However, using synthetic polymer and extensive chemical modification to prepare (DF-PEG) does not involve green chemistry and hinders biomedical applications. Hence, more green approaches should be considered to develop chitosan-based hydrogels for 3D printing without using toxic chemicals, solvents, and extensive modification for clinical applications such as wound healing, tissue engineering, drug delivery, and biosensors applications.

To address these limitations, we have developed a tough and self-healable chitosan-based hydrogel via a green and sustainable approach by taking advantage of the chitosan's inherent cationic nature, enabling chitosan to form a dynamic reversible electrostatic interaction with an anionic polymer. Hence, a dual crosslinked hydrogel via the synergy of horseradish peroxidase (HRP) mediated crosslinking and the phenolated polyelectrolyte complexation (PHEC) between the cationic chitosan and anionic alginate was developed. We hypothesize that the brittleness and rigid structure of the hydrogel resulting from the primary enzymatic crosslinking can be addressed by incorporating weak and reversible electrostatic interactions, as well as in-situ microfiber formation using the PHEC, which is responsible for the toughness and flexibility of the hydrogel as a sacrificial bond for energy dissipation [19-21]. The in-situ microfiber formation is expected to synergistically reinforce the hydrogel mechanical stability and increase the gel viscosity endowing the hydrogel with excellent 3D printability.

Results

The design rationale of the hydrogel

To prepare the phenolated polyelectrolyte complex (PHEC), phenolic compounds were conjugated to the chitosan and alginate backbone by conjugation with 3-(4-hydroxyphenyl) propionic acid (HPA) and tyramine, respectively, via carbodiimide coupling chemistry (Figs. S1,2). Moreover, phenolic compounds are required for hydrogel development via enzyme-mediated crosslinking using horseradish peroxidase (HRP) [22]. The formation of chitosan-phenol (Ch-Ph) and alginate-tyramine (Alg-Ty) was confirmed by ^{1}HNMR and UV-Vis spectra of the purified samples (Figs. S1,2). In ^{1}H NMR, the presence of new peaks at around 7 ppm belonging to aromatic protons confirmed the presence of aromatic protons in the structure of the polymers [23]. Similarly, chitosan and alginate have no absorption at 275nm; however, adding a phenolic group to the structure gives Ch-Ph, and Alg-Ty a maximum absorbance at that wavelength of 275 nm [24].

We then developed a series of hydrogels based on Ch-Ph solution, Alg-Ty solution, and the PHEC suspension. To this end, hydrogel precursors containing different concentrations of Ch-Ph or Alg-Ty (Table S1) were mixed with HRP and H_2O_2. HRP is activated by H_2O_2, which catalyzes the oxidation of the phenolic groups in the chitosan or alginate chains, generating two phenoxy radicals in one

catalytic cycle. The phenoxy radicals can subsequently react with each other through a radical coupling reaction resulting in C-C and C-O bonds leading to the formation of single crosslinked chitosan and alginate hydrogel via covalent bonding [22].

For the double crosslinked chitosan alginate hydrogel (DCCA), the Alg-Ty solution was added dropwise to Ch-Ph with a volume ratio of 1:1 under vigorous agitation and multidirectional mixing to obtain a viscous PHEC suspension. Given the difference in the charge density between positively charged amino groups of chitosan and carboxyl groups of alginate, the electrostatic interaction simultaneously occurred upon mixing the two solutions, leading to the formation of polyion complex and subsequently a physically crosslinked weak hydrogel [25]. Vigorous shear agitation of the weak hydrogel led to the breakage of the hydrogel and *in situ* microfibers formation (Fig 1a), resulting in a heterogenous PHEC suspension with significantly higher viscosity (20 times) compared to the Ch-Ph and Alg-Ty solutions (Fig 2a). Generally, polyelectrolyte complex between chitosan and alginate led to the formation of microfibers at acidic and neutral pH, and microparticle at alkaline condition (pH 8.5) and the fibers surface charge undergoes a transition from positive to the negative surface by increasing the pH from acidic (pH 3.5) to alkaline condition (pH 8.5) [26]. Indeed, instantaneous complexation led to a microfibrous colloidal suspension with hierarchical morphology with micron-scale fibers branching into ever thinner fibers at natural pH (Fig 1a).

Interestingly, we hypothesized that the surface of the in-situ microfibers are functionalized with phenol groups, allowing the microfibers to participate in the enzyme-mediated crosslinking with each other and the phenolated chitosan and alginate (Fig 1b). Then, the PEC suspension with different concentrations of Ch-Ph and Alg-Ty (Table S1) was used for the hydrogel formation via the enzyme-mediated crosslinking using HRP and H_2O_2. The gelation time was determined using the vial tilting method; all hydrogels exhibited a concentration-dependent gelation time (Fig S4b) with a controllable sol-gel transition from approximately two min to a few seconds, indicating that the polymer (phenol group) concentration significantly affects the gelation time due to availability of higher phenolic groups for the enzyme-mediated crosslinking [27]. Although the in-situ microfiber formation increased the viscosity of the gel precursors, the gelation time of hydrogels were not affected by this phenomenon

(Table S1, Fig 4b). These results suggested that the PHEC formation did not influence the velocity of the HRP-catalyzed crosslinking reaction and phenol groups mobility [28]. Hence, the electrostatic interaction did not interfere with the HRP mediated cross-linking. Finally, $Ch_{1.5}$ (named Ch), $Alg_{1.5}$ (named Alg), and a dual crosslinked $Ch_{1.5}$-$Alg_{1.5}$ hydrogel (named DCCA) presenting the shortest gelation time were chosen for further characterization to examine the effect of PHEC on the mechanical properties of the hydrogels.

Physiochemical characterization

Before investigating the PHEC effect on the viscoelastic properties, the PHEC formation was investigated by FTIR (Fig S5) and XRD (Fig S6) on freeze-dried Ch, Alg, and DCCA hydrogels. Both Ch and Alg hydrogels demonstrated typical FTIR bands of the polymers (Fig. S5). The DCCA hydrogel showed a similar spectrum to the Ch and Alg; however, the amide I peak of Ch was disappeared and showed a new sharp peak overlapping with carboxylate groups of alginate at 1567 Cm^{-1} which was shifted from 1557 Cm^{-1} in Alg spectra. Moreover, the carboxylate stretch peak of Alg shifted from 1397 to 1406 after the PHEC formation. These shifts in assigned bands of alginate carboxylic groups and chitosan amino groups could account for the electrostatic formation [25]. Furthermore, the XRD pattern of the freeze-dried hydrogels, chitosan, and alginate powder revealed that phenol modification of chitosan and alginate reduced the intensity of semicrystalline peaks of chitosan and alginate (at around 12° and 20°).

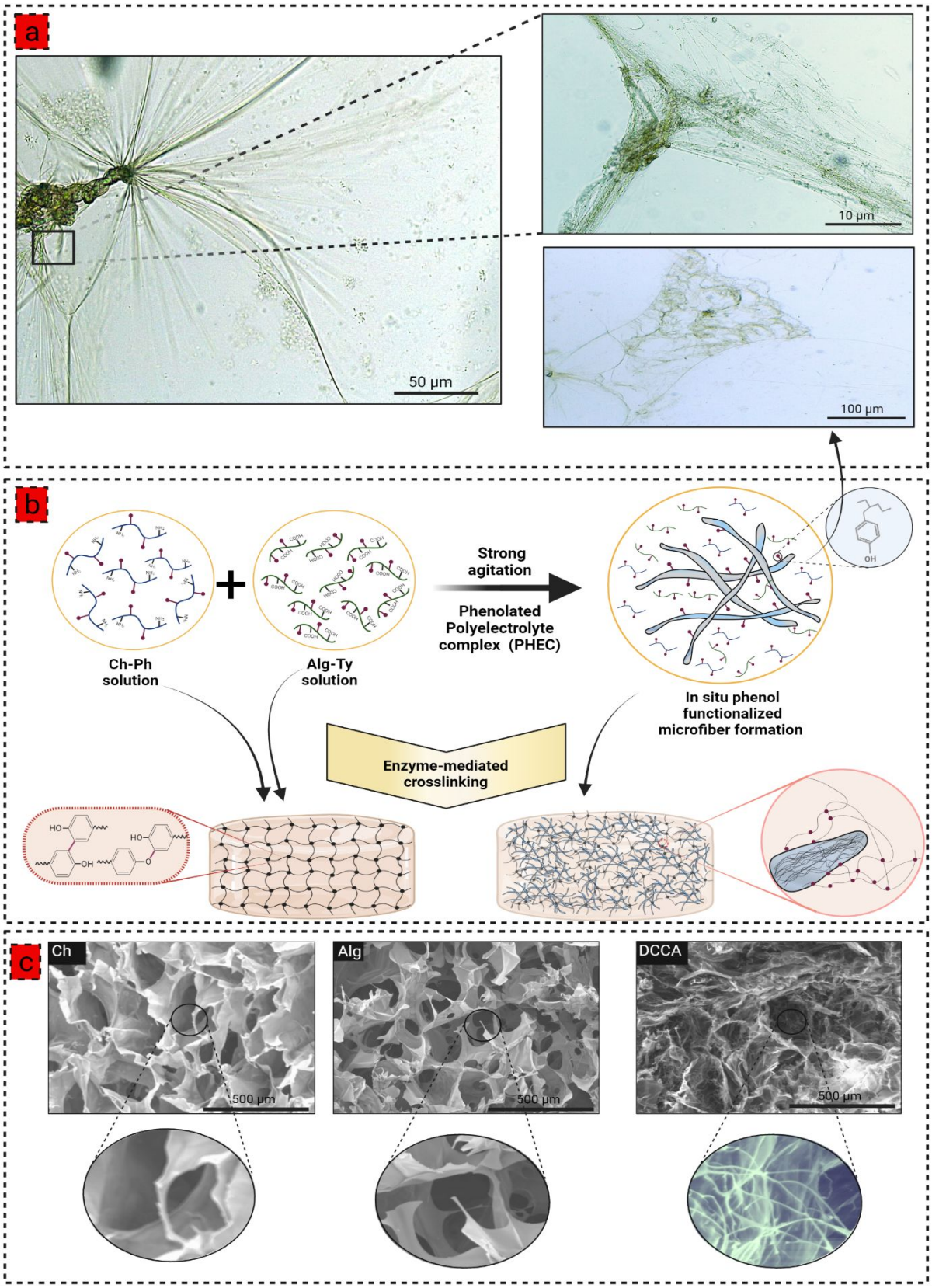

Fig.1 a) Optical microscopy images of *in situ* phenol functionalized microfiber formation by phenolated polyelectrolyte complex (PHEC), showing a hierarchical morphology of microfibers, b) Schematic illustration of phenol functionalized microfiber formation via the PHEC formation between the Ch-Ph and Alg-Ty solution, and

subsequent hydrogel formation by enzyme-mediated crosslinking using horseradish peroxidase (HRP) and hydrogen peroxide (H_2O_2), c) The scanning electron microscopy (SEM) images of Ch, Alg, and DCCA hydrogels illustrating a compact and heterogenous microstructure of DCCA hydrogel compared to Ch and Alg hydrogels due to formation of in situ phenol functionalized microfibers induced by PHEC; the figure was created with BioRender.com.

This phenomenon could be due to the reduction in the inter-and intramolecular hydrogen bonds of chitosan that reduced the crystallinity, in agreement with the water solubility of chitosan after conjugation [29]. Besides, the peaksμ intensity was further reduced in the DCCA hydrogel, indicating that PHEC formation further decreased the crystallinity due to the formation of electrostatic interactions resulting in the breakage of intermolecular hydrogen bonding [29].

The morphological investigation of the hydrogel showed a typical porous microstructure for Ch and Alg hydrogel with an average pore size of 258±53 μm 297±13μm (Fig 1c). However, due to the in-situ microfiber formation, the DCCA hydrogel exhibited a denser microstructure with a hierarchical morphology containing large pores filled with a fibrous structure distributed throughout the hydrogel. The microfibers possessed an average diameter of 1.3 ± 0.4 μm (Fig 1c), which could reinforce the mechanical properties of the hydrogel [30]. The microstructure investigation demonstrated that the fiber-like structure is preserved, indicating the stability of in situ microfibers upon enzyme-mediated crosslinking even after the freeze-drying process.

We investigated the effect of PEC on the swelling rate and degradation behaviour of the hydrogels. PHEC formation reduced the swelling ratio of Alg hydrogel from 311± 15 % to 47 ± 9 % (Fig. S7). Besides, it prolonged the degradation compared to the Ch and Alg hydrogel in lysozyme solution (Fig. S8) due to the formation of a dense network with a high crosslinking density, which results in a smaller pore size filled with microfibers. The results showed that the PHEC formation could significantly affect the hydrogel's swelling ratio and degradation behaviour.

Viscoelastic properties of hydrogels

We next investigated the effect of complexation on the viscoelastic properties of the hydrogel. We characterized the dynamic viscosity and shear thinning properties of the hydrogel precursors (Fig. 2a). DCCA hydrogel precursor exhibited a 20 times higher dynamic viscosity (6500 mPa.s) compared to the Ch and Alg hydrogel precursors indicating the significant effect of in-situ microfibers on the viscosity of the hydrogel precursors. More importantly, the shear-thinning behaviour of DCCA hydrogel precursors was enhanced due to the dynamic nature of non-covalent electrostatic interaction, which dissociated under the applied shear and subsequent network recovery following the shear removal [31, 32].

We monitored the gelation kinetics via a time sweep test (Fig. 2b). The Ch and Alg hydrogel showed a gelation point at around 40 s. However, the gelation point was not observed for the DCCA hydrogel due to its higher G' than the G" at the beginning, showing a solid-like behaviour expected due to the PHEC formation. However, after initializing the HRP-mediated crosslinking, the G' was further increased up to 12 min, similar to the Ch and Alg hydrogel indicating the solidification of the hydrogels. The G' of the DDCA approached 7.1 kPa, which is 50 times higher than previously reported studies on chitosan and alginate polyelectrolyte complex hydrogel [25, 33]. These data suggest that the enzymatic crosslinking significantly improved the stiffness of the hydrogel. Furthermore, an amplitude sweep test (constant frequency of 0.1 Hz) (Fig. 2c) and a frequency sweep (0,1 to 10Hz, at 1 % strain) (Fig. 2d) were performed to evaluate the viscoelastic properties of the hydrogels. All hydrogels exhibited strain-independent G' and a stable structure up to 200 % strain showing a wide range of linear viscoelastic region (LVR) and confirming the elasticity and stability of the hydrogels [34, 35].

The mean value of G' and G" of hydrogels at the linear viscoelastic region (LVR) are shown in Fig. 2e and f, respectively. The Ch hydrogel showed the highest G' value (7.9 kPa), while the Alg hydrogel exhibited the lowest (2.3 kPa) value. Interestingly, the DCCA hydrogel revealed a high G' (7.1 kPa) without any significant difference from the Ch hydrogel indicating the significant role of microfibers in the stiffness of the hydrogel. Ch and Alg hydrogels showed a G" value of around 7 Pa, while the DCCA hydrogel exhibited a significantly higher G" value of around 370 Pa (Fig 2f). Although G' of DCCA was close to the Ch hydrogel, its G" was 30 times higher than Ch and Alg, indicating significantly higher energy dissipation during the deformation of the DCCA hydrogel. In our previous study, the

addition of silk fibroin with lower G' compared to chitosan significantly lowered the G' of the hydrogel (3 times) [36]. However, in this study, the in-situ microfibers could maintain the hydrogel elasticity in addition to increasing the G" of the DCCA.

The hydrogels' loss factor (Tan δ) was measured from the frequency test at 0.1 Hz, indicating how a material can absorb and dissipate energy in response to deformation [37]. Tan δ for the Ch and Alg hydrogels were around 0.001, indicating that the Ch and Alg hydrogels were highly elastic and brittle , while DCCA hydrogel exhibited a Tan δ of 0.06, showing that the DCCA hydrogel is much more viscous thatn the Ch, and Alg hydrogels which can dissipate energy during the deformation [38].

This phenomenon is due to the synergy of covalent enzymatic crosslinking as a brittle irreversible bond and dynamic non-covalent electrostatic interaction as a weak and recoverable bond [39, 40]. The uniformly distributed microfibers limit the amount of stress accumulation in the structure and therefore acts as sacrificial bonds that enable energy dissipation and improve the resilience of the hydrogel [39, 40]. Hence, the DCCA hydrogels revealed high flexibility and toughness without scarifying the stiffness of the hydrogel thanks to the PHEC and phenol functionalized microfibers without using any synthetic polymer.

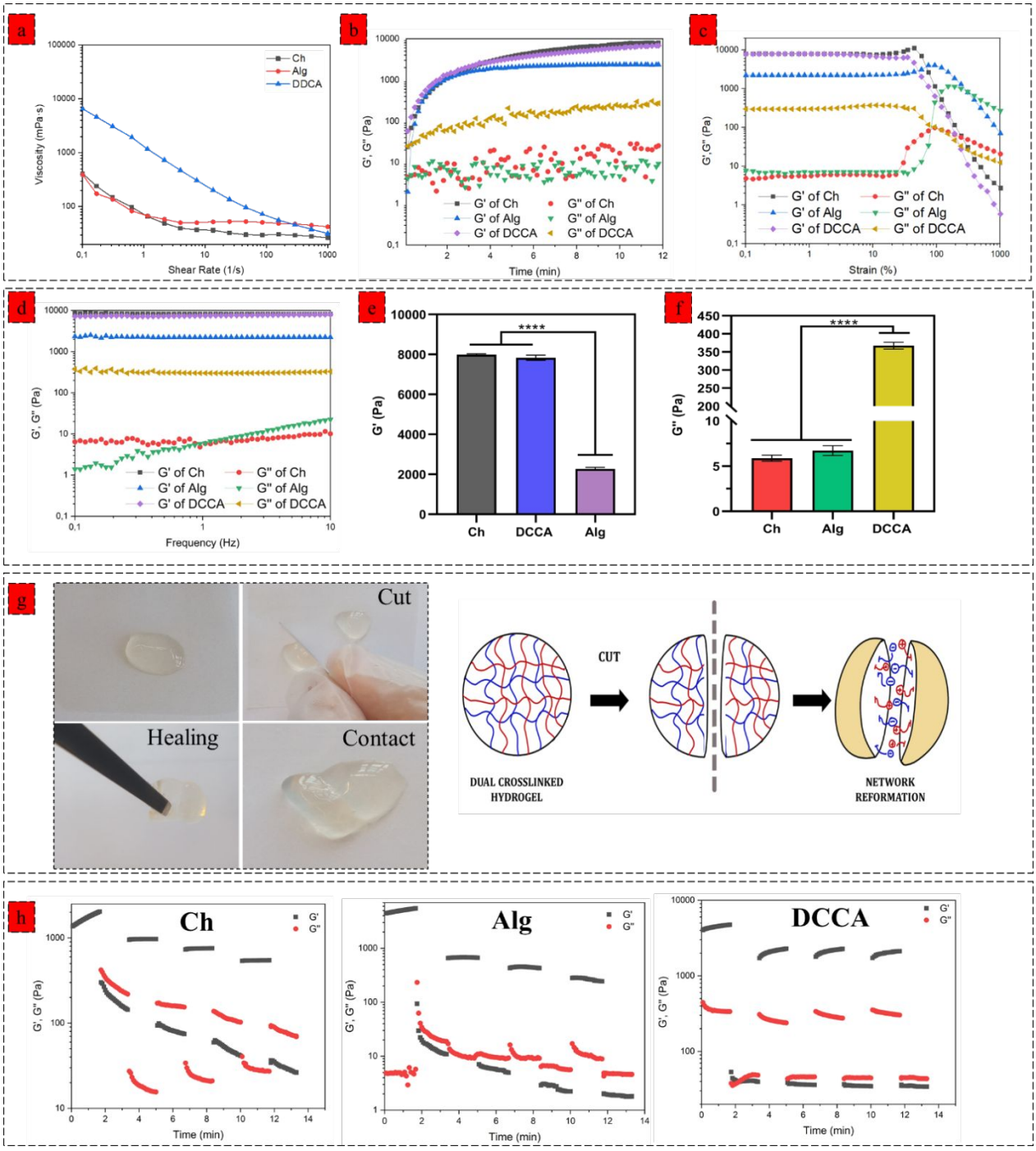

Fig. 2 Rheological properties of the hydrogels. a) shear-rate dependent variations gel precursors viscosity over the shear rate of 0.1-1000 1/s at 37 °C, b) Gelling kinetics of the Ch, Alg and DCCA hydrogel investigated by a time sweep test at a constant strain of 0.1 % and frequency of 1 Hz at 37 °C, c) storage modulus (G') and loss modulus (G")–strain dependence of Ch, Alg and DCCA hydrogels at a constant frequency of 1 Hz at 37 °C, d) G' and G''–frequency dependence Ch, Alg and DCCA hydrogels at a constant strain of 1 % at 37 °C, e) mean value of hydrogels G' at linear viscoelastic region (LVR), f) mean value of hydrogels G" at linear viscoelastic region (LVR), g) macroscopical observation of self-healing behaviour DCCA hydrogel and the self-healing mechanism

of DCCA hydrogels based on the dynamic electrostatic interactions, h) self-healing capability of Ch, Alg and DCCA hydrogels evaluated by 4 cycle step-strain test with 100 s time interval for each step (strain = 1% / 300% /1%...). . Data were analyzed using a one-way ANOVA test. ****p<0.0001.

Self-healing and compression properties of hydrogels

We investigated the effect of complexation on the self-healing property of the hydrogel via macroscopic observations and rheological investigations. The hydrogel was cut into two pieces, and then the two pieces of hydrogels were contacted to examine their self-healing property. After a few minutes, the hydrogel was lifted using a tweezer (Fig. 2g). The two pieces stayed together, showing that new bonding occurred and healed the fractured network. This self-healing capability is due to the interpolymer complex driven by the electrostatic interaction between the negatively charged alginate's carboxyl group and the positively charged chitosan's amino group. The dynamic interaction between these functional groups regenerated upon sealing the gap, showing the reversibility of these interactions [41].

Moreover, a rheological investigation of self-healing properties of Ch, Alg, and DCCA hydrogels was performed (Fig. 2h) using a 4 cycle step-strain test. At each cycle, a 300% strain was applied for 100s to break the gel. The recovery cycle of 100s at a strain of 1% was used to allow the reformation of the network. Both Ch and Alg hydrogels showed a significant reduction in G' (10 times) after the first cycle, indicating that the applied strain damaged the hydrogel network without any recovery due to the presence of only non-dynamic covalent bonds. The DCCA hydrogel showed a complete sol-gel transition during the first interval of 300% strain. Interestingly, after the first cycle, the G' of DCCA was recovered to 2.2 kPa (60 % of initial G') and showed an increasing trend with time, indicating that the DCCA hydrogel could recover the G.' The G' of Ch and Alg decreased continuously after each cycle. The G' values at each cycle were constant, showing the inability of the hydrogel to recover the broken bonds, while DCCA hydrogel could recover 60 % of the G'.

Furthermore, it is worth mentioning that the ascending trend of the G' value of DCCA during the relaxation cycle indicates that the hydrogel probably needs more time to recover the higher amount of the broken bonds. Indeed, the covalent phenolic network of the DCCA hydrogel could preserve the structure from the nonrecoverable damages, while the dynamic chain entanglement and electrostatic

interactions broke quickly and acted as sacrificial bonds to dissipate energy resulting in self-healing ability after the deformation [10]. Furthermore, the loss modulus of DCCA was 30 times higher than for the other hydrogels confirming the previous results regarding the high loss factor representing the toughness and flexible structure of the DCCA hydrogel.

Further examination of the toughness and deformation resistance of the hydrogels was performed using a compression test (Fig 3) by recording the force until the breakage of the hydrogel using a constant pressure (1 mm/min). The compressive strain-stress curve demonstrates the brittleness of the Ch hydrogel compared to Alg and DCCA hydrogels, indicating the brittle and stiff structure of the Ch hydrogel (Fig. 3a). DCCA hydrogel showed the highest fracture strain (55 %) compared to the Ch (41 %) and Alg (48 %) hydrogels. Moreover, an investigation of the compressive modulus of the hydrogels (Fig. 3b) revealed that the DCCA hydrogel exhibited a compressive modulus of 1.37 ± 0.05 kPa without any significant difference compared to Ch hydrogel with the highest modulus (1.51 ± 0.07 kPa). In comparison, Alg hydrogel showed a compressive modulus of 0.43 ± 0.06 kPa, which is in line with the rheological results.

Furthermore, the toughness of the hydrogels indicating their capacity to absorb mechanical energy, was measured by integrating the compressive stress-strain curve[12] (Fig 3c). The DCCA hydrogel showed a significantly higher toughness (13.3 ± 0.9 kJ/m^3) compared to Ch (6.5 ± 0.8 kJ/m^3) and Alg (3.2 ± 0.3 kJ/m^3) hydrogels. Our results showed that the synergistic reinforcement in DCCA hydrogel could increase the hydrogel's toughness and deformability without sacrificing the hydrogel's stiffness. Unlike Ch and Alg hydrogel, the DCCA hydrogel could recover the deformation after the compression, while both Ch and Alg hydrogels were completely broken without any recovery (Fig 3d, Fig 4a). This phenomenon is due to the synergistic complexation induced by PHEC via microfiber formation, which could increase the hydrogel's stiffness and significantly improve the energy dissipation leading to delay in the network fracture [42] (Fig 3e). Hence, the results showed that a straightforward mixing of Ch and Alg hydrogel could significantly improve the toughness and flexibility without requiring additional synthetic polymers.

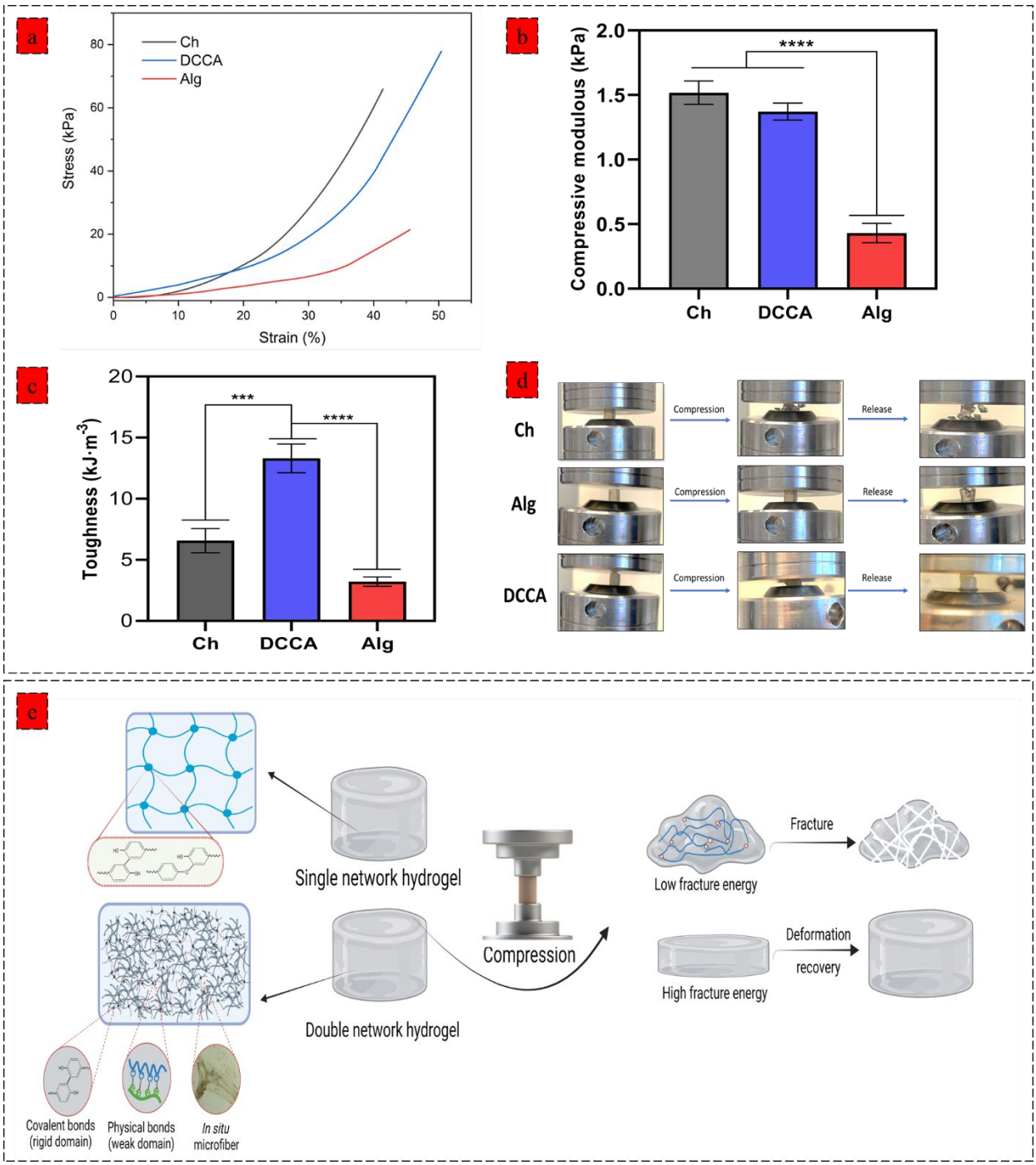

Fig. 3 Mechanical properties of hydrogels. a) compression stress-strain curves of hydrogels, b) compressive modulus of hydrogels calculating from the stress-strain curves (strain 10-15 %), c) the corresponding dissipated energy of hydrogels Data were analyzed using a one-way ANOVA test. ***$p < 0.0005$; ****$p < 0.0001$. d) photographs of Ch, Alg, and DCCA hydrogels showing their compressibility and elasticity under compression, e) schematic illustration of hydrogel deformation recovery after the compression showing destruction of Ch and Alg hydrogel due to their single covalent network and high deformation recovery capability of DCCA hydrogel due

to the synergistic reinforcement effect of PHEC by inducting electrostatic interaction and *in situ* microfibers; the figure was created with BioRender.com.

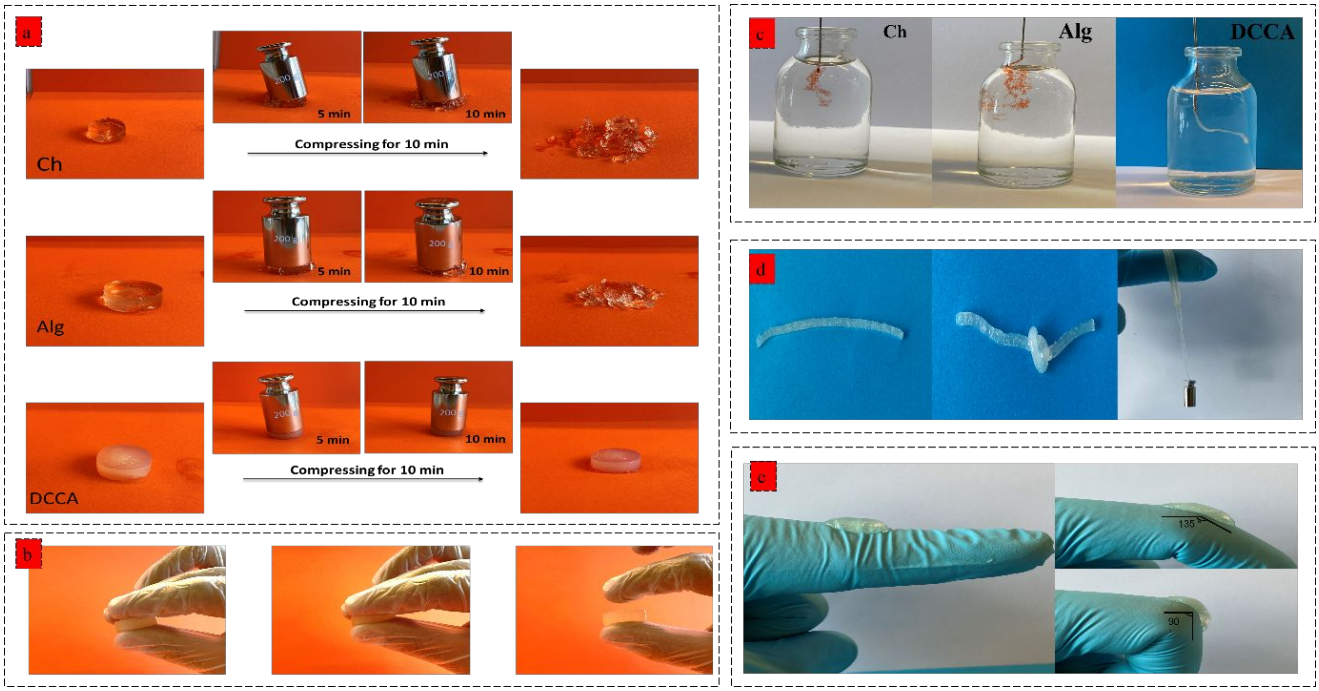

Fig. 4 a) Deformation capability of Ch, Alg and DCCA hydrogels after being pressed by the 200 g weight for 10 min, and b) deformation resistance of DCCA hydrogel by pressing between fingers, c) Injectability of Ch, Alg, and DCCA evaluation using a syringe with 30 G needles, d) foldability and knotting ability of DCCA hydrogel and high mechanical flexibility could sustain a 50 g weight, e) The DCCA hydrogel adherence to a knuckle which was repeatedly bent from 180° to 90° in the flexibility test 50 times to examine the flexibility and adhesion performance.

The hydrogels' injectability was investigated by loading the gel precursors into a syringe and evaluating the injection capability by extruding the gel precursors through a 30 G needle into PBS (Fig. 4b). Both Ch and Alg hydrogels did not show a successful injection into the PBS buffer, and the gel was broken after the injection without any recovery due to the rigid and brittle structure of the hydrogels. However, the DCCA hydrogel could be extruded through the needle due to the presence of weak electrostatic interactions endowing the hydrogel with the self-recovery capability [43]. Indeed, due to the reversible nature of these weak physical interactions, the formed network can be broken and reformed when the shear caused by the injection through the needle was removed [44].

Moreover, the DCCA hydrogel could exhibit good flexibility by knotting the hydrogel and could sustain a 50 g weight for more than 30 min indicating high mechanical strength and flexibility of the hydrogel (Fig. 4d), which was not observed in the Ch and Alg hydrogel due to their brittle and non-reversible covalent bonds. Besides, the adhesive performance of the DCCA hydrogel was tested by bending the hydrogel to a knuckle of more than 50 elongation/recovery cycles (Fig. 4e). During the elongation/recovery cycles, the DCCA hydrogel could maintain its structure while the hydrogel's adhesiveness prevented it from falling off due to the presence of electrostatic interaction between the polymers [45].

Our results demonstrated that DCCA hydrogel has high mechanical strength, toughness, flexibility, and moldability as an injectable hydrogel for clinical applications with a minimally invasive approach for regenerating irregular-shaped defects, particularly wound healing applications. As a biopolymer-based hydrogel without using any synthetic polymer or harmful crosslinking agent, the approach used in this study could open new insight into the design and development of bio-based hydrogels for biomedical applications.

Biological properties

We evaluated the hydrogels' biological activity to examine the effect of PHEC on the antioxidant, antibacterial, and cell proliferation capacity of the hydrogel. The DPPH scavenging evaluation (Fig. 5a) revealed a scavenging activity of 51.3 ±3.5 % for Ch, 37.9 ± 2.6 % for Alg and 44.4 ± 6.4% for DCCA, demonstrating that the PHEC formation did not have any significant effect ($P < 0.05$) on the inherent antioxidant activity of chitosan.

Furthermore, the antibacterial activity of Ch, Alg and DCCA hydrogels was investigated by an inhibition test against *S.aureus* (Fig. 5b) and *E.Coli* (Fig. 5c) growth via measuring the optical density (OD) of a bacterial suspension at 600 nm, as well disk diffusion test (Fig. 5d). The Alg hydrogel did not show any inhibition activity against both gram-negative and positive bacteria. The OD of bacteria suspension treated with Alg hydrogel did not show any significant difference compared to the control groups demonstrating no antibacterial activity of the Alg hydrogel [46]. However, the Ch hydrogel

exhibited growth inhibition against both gram-negative and positive bacteria with a mean OD of 0.11 ± 0.02 and 0.14 ± 0.01 against *E.Coli* and *S.aureus*, respectively.

The results showed that Ch hydrogel demonstrated a higher antibacterial activity against *E.Coli* probably due to its cationic nature enabling chitosan to have more antibacterial activity against gram-negative bacteria [47]. DCCA had lower antibacterial activity than the Ch hydrogel; however, the OD of bacterial suspension treated by DCCA hydrogels is significantly lower than the control groups against *E.Coli* (0.2 ± 0.004) and *S.aureus* (0.22± 0.02). Similar to the inhibition growth test, the disk diffusion test, carried out to further investigate the antibacterial activity of the hydrogels, showed no inhibition zone for the Alg hydrogels. However, an inhibition zone was observed for Ch and DCCA hydrogels against both strains of bacteria, which indicated the bactericidal activities of the hydrogels. On the other hand, due to the use of similar H_2O_2 concentrations for all the hydrogels and because alginate has no antibacterial activity, it was confirmed that H_2O_2 did not have any effect on the antibacterial activity of Ch, and the DCCA hydrogel. Hence, these results revealed that the DCCA hydrogel has antibacterial activity due to the presence of chitosan with inherent microbiocidal properties. Indeed, two antibacterial activity mechanisms can be considered for chitosan-based material. Positively charged chitosan would interact with the negatively charged microbial cell wall [48]. For *E.Coli* (gram-negative), the bacteria possess an outer covering of phospholipids and lipopolysaccharides, leading to a negatively charged surface. The interaction between chitosan and the microbial cell wall leads to leakage of proteinaceous and other intracellular constituents. The second factor is the bonding of chitosan with the DNA of bacteria, resulting in the prevention of transcription and translation by DNA [48, 49].

We further investigated the effect of Ch, Alg, and DCCA hydrogels on the viability of 3T3-L1 fibroblasts by a direct contact test using an MTS assay after 24 and 72 h of culture (Fig. 5e). No significant effect on the cell viability of 3T3-L1 was observed for the hydrogels compared to the control (cell culture media) (p <0.05). To further investigate the cell encapsulation capability of hydrogels, 3D encapsulation of 3T3-L1 fibroblast cells into Ch, Alg, and DCCA hydrogels was performed, and the cell nucleus spreading distribution as well as cell viability was evaluated via Hoescht/ethidium bromide staining (Fig. 5f). A uniform spreading distribution of 3T3-L1 fibroblast cells encapsulated into

hydrogels was observed after 1 and 3 days of culture, showing the capability of the hydrogels for homogenous cell spreading and proliferation with a low amount of dead cells (stained with ethidium bromide) compared to the live cells (stained by Hoescht). The results indicate that the PHEC formation in the DCCA hydrogel did not adversely affect biological activities. This hydrogel with toughness and flexibility is a promising candidate for 3D cell encapsulation for various biomedical applications such as cell and gene delivery, regenerative medicine, and wound healing.

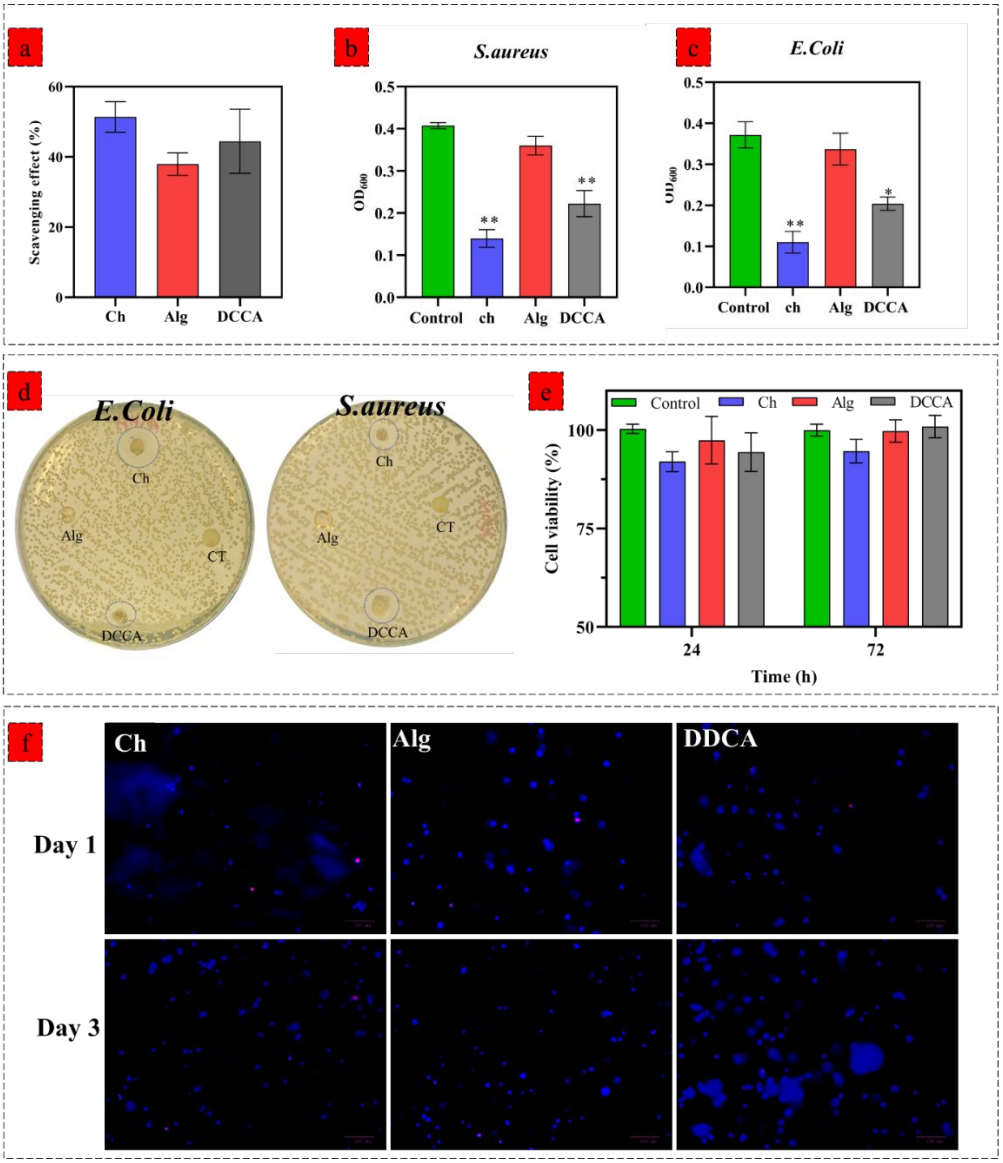

Fig. 5 a) DDPH scavenging effect of Ch, Alg and DCCA hydrogels, results are expressed as % scavenging activity and are the mean ± SD of three independent experiments, b, c) bacterial growth of E. Coli (*b*) and S. aureus (*c*) treaded by Ch, Alg, and DCCA hydrogels after 24 h incubation at 37 °C, results are expressed as optical density (OD_{600}) and are the mean ± SD of three independent experiments, Data were analyzed using a one-way ANOVA test. **p* < 0.05, ***p* <0.005, b) Zone inhibition investigation of *E. coli* and *S. aureus* treated by Ch, Alg, and DCCA hydrogels, e) Cell viability of 3T3-L1 cells seeded on the Ch, Alg, and DCCA hydrogels for 24 and 72 h. Results are expressed as % cell viability and are the mean ± SD of three independent experiments. Data were analyzed using a one-way ANOVA test. **p* < 0.05 as compared to the control (cell culture media), f) Fluorescent microscopic images of cell-laden Ch, Alg, and DCCA hydrogels. The 3T3l fibroblast was encapsulated into cell-laden hydrogels and was stained via Hoescht and ethidium bromide (dead cells) after 1 and 3 days.

3D printing

By using a synergistic complexation approach, the properties of the mixture can be precisely controlled to facilitate 3D printing via extrusion, which has traditionally been difficult with hydrogel precursors. For printing of the DCCA hydrogel, we investigated the effect of a higher concentration (2-4 %) of PHEC suspension on the printability of the hydrogel. Viscoelastic properties of PHEC suspension (2, 2.5, 3, 3.5, and 4 %) were determined, and the results demonstrated that the PHEC suspension with a concentration of 2% had an inadequate viscosity (10 Pa·s) at a shear rate of 0.1 1/s (Fig. S9a) and was still in the sol-phase (G'=50 Pa, and G''= 80 Pa) at 1 % strain according to the amplitude test (Fig. S9b) which is not suitable for 3D printing [50]. However, by increasing the PHEC concentration to 2.5%, the suspension exhibited a solid-like behaviour (G'=122 Pa, and G''= 70 Pa) (Fig. S10b) with a higher viscosity (17 Pa·s) (Fig. S10a). Indeed, increasing the PHEC concentration led to a higher amount of in-situ microfibers with self-assembly features, resulting in the formation of instantaneous solid-like hydrogel upon the addition of phenolated alginate to phenolated chitosan solution (Video S1, PHEC 3%). Finally, the PHEC suspension with 4% concentration was chosen for 3D printing. It is worth mentioning that no Ch-Ph, Alg-Ty, nor non-phenolated polyelectrolyte complex (PEC) can be used alone as a printing ink at the same concentration of PHEC (4%). As mentioned above, the dynamic viscosity of Ch-Ph, Alg-Ty was not high enough to be printed. On the other hand, we evaluated the viscosity of PEC (Fig. 6b) to examine the effect of phenol modification on the viscoelasticity of the hydrogel precursor. PEC possessed a viscosity of 41 Pa.s, which was twice lower than the viscosity of PHEC (110 Pa.s), indicating the significant effect of chitosan and alginate phenol modification in increasing the viscosity of the gel precursor (Video S2). This phenomenon can be explained by the formation of hydrophobic interactions between the side groups (phenyl groups) of chitosan and alginate, leading to a significant increase in the viscosity of phenolated PEC compared to its non-phenolated counterpart [51]. Furthermore, the amplitude sweep test revealed (Fig. 6c) the insufficient stiffness of PEC as standalone ink due to its low G' (50 Pa) compared to the G" (43 Pa) at the strain of 0.1 %. However, PHEC possessed a solid-like network with 24 times higher G' (1200 Pa) compared to the non-phenolated one due to the synergy of electrostatic and hydrophobic interaction at low strain (< 1%) and

by increasing the strain beyond the yield point, sol-like behaviour was observed resulting in the extruding ability of the PHEC suspension.

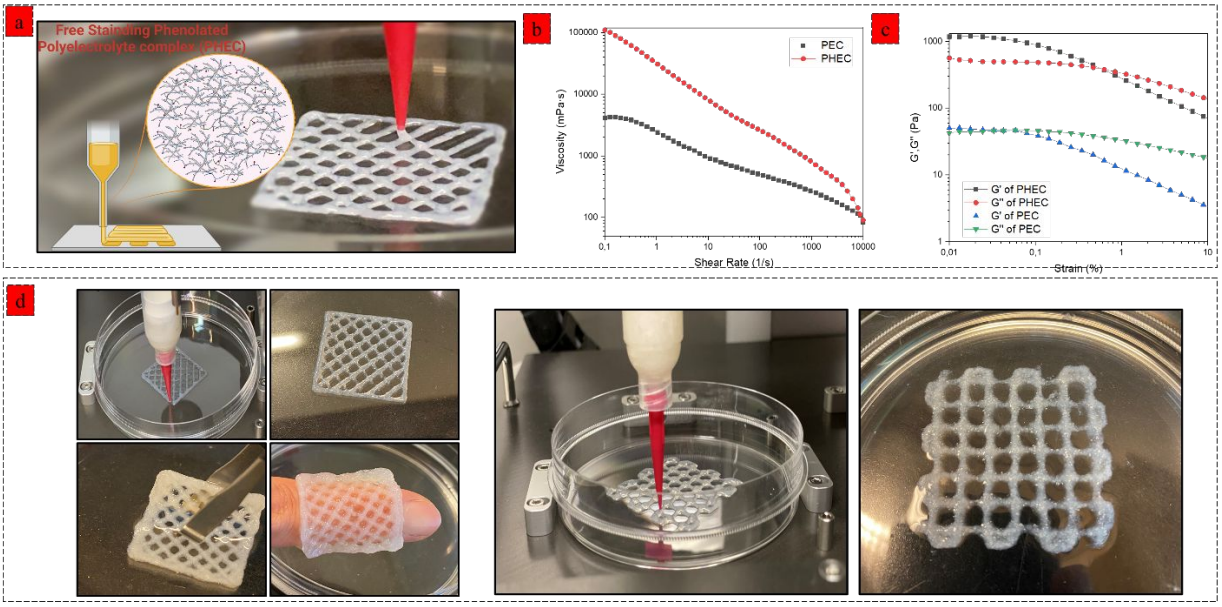

Fig. 6 3D printing with phenolated polyelectrolyte complex (PHEC) hydrogels. a) Schematic illustration and image of 3D printing of PHEC, the figure was created with BioRender.com. b) shear-rate dependent dynamic viscosity of PHEC and non-phenolated over the shear rate of 0.1-1000 1/s, c) storage modulus (G') and loss modulus (G")–strain dependence of phenolated PEC and non-phenolated PEC at a constant frequency of 1 Hz at 37°C, d) Images of extruded PHEC (4%) that has been layered in a 3D structure.

The 3D printing process of the phenolated PEC hydrogel was performed using a bioplotter pneumatic dispensing system (BioScaffolder 3.1, GeSiM, Germany) (Fig. 6a). PHEC suspension was extruded via an 18 G plastic needle (diameter: 250µm) at 140 kPa with a speed of 11 $mm \cdot s^{-1,}$ and the gel retained its shape neatly after extrusion due to its reversible non-dynamic bonds (Video S3). Several examples of 3D-printed hydrogels are shown in Fig. 6d. The extrusion rate of the hydrogel was not slowed, even after adding more than 7 layers of the hydrogel. For further solidification, the 3D printed hydrogels containing HRP (1 U/mL) were soaked in diluted H_2O_2 solution (5 mM) for 5 min to increase the hydrogels' stiffness through mild and nontoxic enzymatic crosslinking of phenol groups presented on the microfibers surface, chitosan, and alginate chain which enables for 3D encapsulation of cells and bioactive agent [52].

Discussion

We introduced a new class of printable hydrogel reinforced by the synergistic effect of phenolated polyelectrolyte complex (PHEC) between phenolated chitosan and alginate chains. The complexation not only enables the 3D printability of the hydrogel but also significantly improves the toughness, moldability, flexibility, and self-healing capacity of the hydrogel. Indeed, PHEC self-induced reinforcement by in-situ microfiber formation between positively charged phenolated chitosan and negatively charged phenolated chitosan led to a significant increase in the suspension's viscosity. On the other hand, increasing the concentration of PHEC beyond 2.5 % (Ch-Ph, and Alg-Ty 2.5 %) endowed the PHEC suspension with adequate viscosity and solid-like behaviour necessary for 3D printing without the addition of any other compound and free of extensive chemical modification. This phenolated polyelectrolyte complex was prepared using chitosan and alginate, and this principle can be applied to a wide range of combinations of phenolated cationic and anionic biopolymers indicating the broad applicability of this method. While various 3D printing methods such as ionic crosslinking or photo-crosslinking of alginate and chitosan-based hydrogels have been reported previously [18, 53-55], there are several advantages in using the proposed method, such as high flexibility, toughness, and foldability of the hydrogel due to the in situ microfiber formation and weak physical interaction leading to increase the energy dissipation. Besides, the PHEC suspension shows tunable concentration-dependent viscoelastic properties from sol to solid-like behaviour due to the rapid physical solidification (Video S1) between the microfibers via hydrophobic, electrostatic, and van der Waals interactions. The dynamic nature of these reactions allows for easy extrusion and injection as a crucial requirement of hydrogels for 3D printing applications. The PHEC approach can be an efficient solution for common hydrogel inks with low yield stress to improve the extrusion capability.

Our novel 3D printable PHEC hydrogels exhibited superior properties compared to the recent 3D printable biobased hydrogel. For example, a recent study showed that incorporating alginate soft dendritic colloids into an alginate solution could endow the hydrogel with 3D printability [56]. However, due to the low stiffness and long solidification time (60 min), the hydrogel formation required additional ionic crosslinking, hampering its biomedical applicability. Alternatively, another recent study reported

a 3D printable polyelectrolyte complex between alginate and ε-polylysine. However, a high concentration of alginate (40 %) and ε-polylysine (~ 30%) was required to reach an adequate viscosity, and additional ionic crosslinking was needed for further solidification [57].

In contrast, our new bioink showed adequate physical stability required for 3D printability at a much lower concentration (2.5 % polymers) due to the synergistic effect of PHEC. Furthermore, in contrast to typical chitosan and alginate 3D printed hydrogels, our 3D printed hydrogel possesses greater flexibility and foldability, thanks to the synergistic reinforcement by in-situ microfiber formation (Video S4). Besides, the phenol modification can endow the 3D printed hydrogel with photo-crosslinking capability using visible light as a safe and biocompatible method, further providing a suitable substrate for 3D cell encapsulation and bioink development [18]. Hence, this work employed natural marine resources to fabricate 3D printable hydrogels using green chemistry technology. Indeed, we showed that the phenolated polyelectrolyte complex as a new concept could be formed between phenolated alginate and chitosan close to neutral pH without the use of acidic media compared to the previously described polyelectrolyte complex between chitosan and alginate [26, 58]. Moreover, further modification, such as oxidation of phenolated alginate, can be performed to increase the hydrogel's self-healing efficacy by introducing reversible imine bonds. Furthermore, tuneable viscoelasticity of the double crosslinked hydrogel can be optimized to promote fundamental cell processes and behaviours dependent on the matrix's viscoelasticity [59]. We believe that the proposed method described in this study offers a green approach for the 3D printing of chitosan-based hydrogels for biomedical applications, such as biomaterials [60], biosensors [61], food applications [62], and personalized medicine [63].

Materials and Methods

Materials

Chitosan with a deacetylation degree ≥75 %, sodium alginate (9005-38-3), 1-ethyl-3-(3dimethylaminopropyl)carbodiimide (EDC) (98 %), N-hydroxysuccinimide (NHS) (98 %), horseradish peroxidase (HRP) (Type VI, essentially salt-free, lyophilized powder, ≥250 units/mg solid), sodium chloride, hydrogen peroxide (H_2O_2) (30 %), 4-Morpholineethanesulfonic acid, 2-(N-Morpholino)ethanesulfonic acid (MES), Hoechst (H33342) and ethidium homodimer I (EH1) (E1903) were purchased from Sigma Aldrich (St. Louis, MO, USA). 3-(4-Hydroxyphenyl) propionic acid (>98 %) and tyramine hydrochloride (>98 %) were obtained from Carbosynth (Compton, United Kingdom).

Fabrication and characterization of phenolated chitosan and alginate

Chitosan and alginate were conjugated with phenol groups via carbodiimide coupling chemistry using 3-(4-hydroxyphenyl) propionic acid (HPA) and tyramine hydrochloride, respectively [64, 65]. Briefly, 1 g (6 mmol) of 3-(4-hydroxyphenyl) propionic acid (HPA) was dissolved in 20 mL aqueous ethanol (50 % v/v), then 0.5 g (3 mmol) EDC was added to the solution, followed by the addition of 0.3 g NHS (2.6 mmol) and allowed to stir at 25 °C for 30 min. The resulting solution was added dropwise to a 100 mL 1 wt% chitosan (solubilized in diluted HCl solution) at the pH of 4.75. The pH of the solution was kept at 4.75 by the dropwise addition of 1 M HCl. After 24 h stirring at 25 °C, the solution was dialyzed against 4.5 L of NaCl solution (0.6 %) at pH 4.5 for 3 days with changing the dialysis solution every 8 h. Then the sample was dialyzed against distilled water for another 4 h, and the resulting dialysate was freeze-dried for 48 h and kept in a moisture-free desiccator before use.

For the alginate modification, Briefly, 0.5 g (3 mmol) EDC and 0.3 g (2.6 mol) of NHS were added to a solution of 1 g of sodium alginate dissolved in 100 ml of MES (2-(N-morpholino)ethanesulfonic acid) buffer (50 mM), and the pH was adjusted to 6 by 1 M NaOH. Subsequently, 0.7 g (4 mmol) tyramine hydrochloride dissolved in 20 ml of MES (50 mM) was added dropwise to the alginate solution and continuously stirred for 24 h at 25 °C. The solution was dialyzed against distilled water for three days with changes of water every 8 h. The final product was freeze-dried and kept in a moisture-free

desiccator prior to use. The modification of phenolic groups on the chitosan and alginate backbones was investigated using ^{1}H NMR and ultraviolet-visible spectroscopy.

Preparation of hydrogel

A series of hydrogels based on chitosan, alginate, and mixtures were prepared in 1 mL vials at 37 °C [66]. To prepare chitosan or alginate hydrogels, different concentrations of Ch-Ph and Alg-Ty (0.5, 1, and 1.5 % w/v) (Table S1) were dissolved in PBS (pH 7.4). The gelation was performed using two vial methods; one vial containing 90µL of the polymers (Ch-Ph or Alg-Ty) and 10µL of HRP (0.1 mg/mL), while the other containing 90µL of the polymers and 10µL of H_2O_2 was then mixed and gently stirred to homogenize the solution and allow subsequent gel formation. The gelation time was recorded by the tube inversion method. The final concentration of HRP and H_2O_2 was 1 U/mL and 1 mM, respectively.

To prepare the mixture hydrogels, different combinations (Table S1) of Ch-Ph and Alg-Ty were prepared by dissolving Ch-Ph in deionized water at pH 6.5 and Alg-Ty in deionized water at pH 8 to make sure that the amino groups of chitosan and carboxylic acid groups of alginate are in the form of protonated, and deprotonated, respectively. Then, the Alg-Ty solution was dropwise added to the Ch-Ph solution with a volume ratio of 1:1, and the mixture was vigorously stirred with a magnetic stirring to allow homogenization of the PHEC suspension. After the homogenization, the hydrogel formation and gelation time measurement were performed similarly on the individual chitosan and alginate hydrogels.

Characterization

The infrared spectra of freeze-dried hydrogels were recorded using an FT/IR-6600 FT-IR Spectrometer (JASCO, Japan) with a resolution of 4 cm^{-1} and 64 scans per spectrum. High-resolution X-ray diffraction (XRD) analysis was performed using an X-Ray Diffractometer (XRD; Bruker ecoD8 advance). The microporous structure of the hydrogel was investigated using scanning electron microscopy (HITACHI, SU-70, Japan). The average pore size and the microfiber diameter were analyzed using Image J software (version 1.53k, National Institutes of Health, Bethesda, MD,

USA).The hydrogels' swelling ratio and degradation rate were evaluated by the gravimetric method in PBS and lysozyme solution at 37 °C, respectively. Details are described in Supplementary Notes 1-2

Rheological and compression characterization of hydrogels

The rheological properties were investigated in a rheometer (Modular Compact Rheometer MCR 302, Anton Paar, Austria) coupled with a parallel plate (25mm, and 0.5 mm gap size) with the temperature maintained at 37 °C for all experiments. The hydrogel precursors' dynamic viscosity was measured via the flowability test over a range of shear rates (0.1-10000 1/s). Hydrogels' gelation kinetics was investigated by a time sweep oscillatory test at a constant frequency of 1 Hz and a strain of 0.1 % (LVR). The frequency sweep test was carried out over the frequency range of 0.1 to 10 Hz at a constant strain of 1 %. Amplitude sweep ranged from 0.01 to 1000 % strain was performed at a constant frequency of 1 Hz to determine the linear viscoelastic region (LVR).

The compression properties of the hydrogels were evaluated using a Zwick/Roell Z020 universal testing machine (Zwick GmbH, Ulm, Germany) with 2K N cell load. Cylindrical hydrogels with a diameter and height of 6 mm were prepared in flat-bottom vials. The compression test was performed with a 1 mm/min crosshead speed, and the stress-strain curves were recorded. The compressive modulus was calculated from the slope of linear stress-strain curves, and the toughness was measured by integration of stress-strain curves using OriginPro (9.6.5.169).

Antioxidant and antibacterial activity

DPPH[1] radical scavenging assay was performed to investigate the antioxidant activity of hydrogels according to a previously reported method [66]. The antibacterial activity of the hydrogels against gram-negative bacteria *E.Coli* and gram-positive bacteria *S.aureus* were investigated using the growth inhibition assay [67] and disk diffusion test [68]. Details are described in Supplementary Notes 3-4.

[1] 2,2-diphenyl-1-picryl-hydrazyl-hydrate

3D Cell encapsulation and biocompatibility evaluation

The cytocompatibility of hydrogels was investigated using CellTiter 96® AQ_{ueous} One Solution Cell Proliferation Assay (MTS, Promega) and live/dead staining using Hoechst 33,342/PI double-staining assay. 3T3-L1 cells were seeded on the hydrogels at a density of 5×10^3 cells/well and incubated for three days, and the media was replaced every day. The cytotoxicity of the hydrogels was evaluated on days 1, and 3 using an MTS assay. For 3D cell encapsulation, sterile gel precursors containing 3T3-L1 cell suspension with a cell density of 5×10^5 cells/mL were used to form the hydrogels in a Millicell EZ SLIDE 8-well glass (Merck, Kenilworth, NJ, USA) followed by 30 min incubation at 37 °C prior to culture. After 1 and 3 days of culture, the encapsulated cell was stained using Hoechst/ethidium homodimer I (EH1) staining. Details are described in Supplementary Notes 5.

Statistical analysis

All experiments were performed in triplicates, and the results were expressed as means ± standard deviations (SD). Statistical analyses were performed using GraphPad Prism 8 (GraphPad Software Inc.) using either one-way ANOVA or two-way ANOVA followed by Bonferroni's post hoc test. P-values < 0.05 were considered statistically significant. Wherever significance has been proven, it is indicated by $*p < 0.05$; $**p < 0.005$; $***p < 0.0005$; $****p < 0.0001$.

Declaration of Competing Interest

The authors declare no conflict of interest.

Acknowledgments

H.J and A.S. acknowledge funding from Innoviris Brussels, Belgium (https://innoviris.brussels) under the project 2019 – BRIDGE – 4: RE4BRU. The content is solely the responsibility of the authors and does not necessarily represent the official views of the above-mentioned funding agency. The authors would like to thank Dr. Véronique Fontaine for her assistance with the antibacterial test.

References

1. Q. V. Nguyen, J. H. Park and D. S. Lee, *European Polymer Journal*, 2015, **72**, 602-619.
2. J.-Y. Sun, X. Zhao, W. R. Illeperuma, O. Chaudhuri, K. H. Oh, D. J. Mooney, J. J. Vlassak and Z. Suo, *Nature*, 2012, **489**, 133-136.
3. Y. Huang, D. R. King, T. L. Sun, T. Nonoyama, T. Kurokawa, T. Nakajima and J. P. Gong, *Advanced functional materials*, 2017, **27**, 1605350.
4. D. Zhao, J. Huang, Y. Zhong, K. Li, L. Zhang and J. Cai, *Advanced Functional Materials*, 2016, **26**, 6279-6287.
5. S. Xia, S. Song and G. Gao, *Chemical Engineering Journal*, 2018, **354**, 817-824.
6. T. Zhu, J. Mao, Y. Cheng, H. Liu, L. Lv, M. Ge, S. Li, J. Huang, Z. Chen and H. Li, *Advanced Materials Interfaces*, 2019, **6**, 1900761.
7. I.-Y. Kim, S.-J. Seo, H.-S. Moon, M.-K. Yoo, I.-Y. Park, B.-C. Kim and C.-S. Cho, *Biotechnology advances*, 2008, **26**, 1-21.
8. F. Croisier and C. Jérôme, *European polymer journal*, 2013, **49**, 780-792.
9. M. Rajabi, M. McConnell, J. Cabral and M. A. Ali, *Carbohydrate Polymers*, 2021, 117768.
10. C. Cui, C. Shao, L. Meng and J. Yang, *ACS applied materials & interfaces*, 2019, **11**, 39228-39237.
11. J. Liu, B. Yang, M. Li, J. Li and Y. Wan, *Carbohydrate polymers*, 2020, **227**, 115335.
12. H. Y. Jung, P. Le Thi, K.-H. HwangBo, J. W. Bae and K. D. Park, *Carbohydrate Polymers*, 2021, **261**, 117810.
13. C. Xu, W. Zhan, X. Tang, F. Mo, L. Fu and B. Lin, *Polymer testing*, 2018, **66**, 155-163.
14. M. C. Pellá, M. K. Lima-Tenório, E. T. Tenório-Neto, M. R. Guilherme, E. C. Muniz and A. F. Rubira, *Carbohydrate Polymers*, 2018, **196**, 233-245.
15. J. You, S. Xie, J. Cao, H. Ge, M. Xu, L. Zhang and J. Zhou, *Macromolecules*, 2016, **49**, 1049-1059.
16. Q. Wu, M. Maire, S. Lerouge, D. Therriault and M. C. Heuzey, *Advanced Biosystems*, 2017, **1**, 1700058.
17. L. Zhou, H. Ramezani, M. Sun, M. Xie, J. Nie, S. Lv, J. Cai, J. Fu and Y. He, *Biomaterials Science*, 2020, **8**, 5020-5028.
18. Y. Liu, C.-W. Wong, S.-W. Chang and S.-h. Hsu, *Acta Biomaterialia*, 2021, **122**, 211-219.
19. J. Berger, M. Reist, J. M. Mayer, O. Felt and R. Gurny, *European journal of pharmaceutics and biopharmaceutics*, 2004, **57**, 35-52.
20. W. Pu, F. Jiang, P. Chen and B. Wei, *Soft Matter*, 2017, **13**, 5645-5648.
21. H. Fan, J. Wang, Z. Tao, J. Huang, P. Rao, T. Kurokawa and J. P. Gong, *Nature communications*, 2019, **10**, 1-8.
22. S. Sakai and M. Nakahata, *Chemistry–An Asian Journal*, 2017, **12**, 3098-3109.
23. M. H. Kim, J. N. Lee, J. Lee, H. Lee and W. H. Park, *ACS Biomaterials Science & Engineering*, 2020, **6**, 3103-3113.
24. Y. Zhong, J. Wang, Z. Yuan, Y. Wang, Z. Xi, L. Li, Z. Liu and X. Guo, *Colloids and Surfaces B: Biointerfaces*, 2019, **179**, 462-469.
25. D. Komoto, T. Furuike and H. Tamura, *International journal of biological macromolecules*, 2019, **126**, 54-59.
26. G. K. Wasupalli and D. Verma, *International journal of biological macromolecules*, 2018, **114**, 10-17.
27. R. Jin, C. Lin and A. Cao, *Polymer Chemistry*, 2014, **5**, 391-398.
28. T. T. H. Thi, Y. Lee, S. B. Ryu, H.-J. Sung and K. D. Park, *RSC advances*, 2017, **7**, 34053-34062.
29. Y. Wang, M. Xie, G. Ma, Y. Fang, W. Yang, N. Ma, D. Fang, Q. Hu and F. Pei, *Carbohydrate polymers*, 2019, **225**, 115238.

30. M. de Ruijter, A. Hrynevich, J. N. Haigh, G. Hochleitner, M. Castilho, J. Groll, J. Malda and P. D. Dalton, *Small*, 2018, **14**, 1702773.
31. S. Uman, A. Dhand and J. A. Burdick, *Journal of Applied Polymer Science*, 2020, **137**, 48668.
32. M. Truong and L. Walker, *Langmuir*, 2002, **18**, 2024-2031.
33. X. Lv, Y. Liu, S. Song, C. Tong, X. Shi, Y. Zhao, J. Zhang and M. Hou, *Carbohydrate polymers*, 2019, **205**, 312-321.
34. R. Jin, C. Hiemstra, Z. Zhong and J. Feijen, *Biomaterials*, 2007, **28**, 2791-2800.
35. S. V. Gohil, S. B. Brittain, H.-M. Kan, H. Drissi, D. W. Rowe and L. S. Nair, *Journal of Materials Chemistry B*, 2015, **3**, 5511-5522.
36. H. Jafari, A. Dadashzadeh, S. Moghassemi, P. Zahedi, C. A. Amorim and A. Shavandi, *Gels*, 2021, **7**, 138.
37. O. Yuksel, M. Sandberg, I. Baran, N. Ersoy, J. H. Hattel and R. Akkerman, *Composites Part B: Engineering*, 2021, **207**, 108543.
38. O. Okay and W. Oppermann, *Macromolecules*, 2007, **40**, 3378-3387.
39. M. Sun, J. Qiu, C. Lu, S. Jin, G. Zhang and E. Sakai, *Polymers*, 2020, **12**, 2263.
40. S. Talebian, M. Mehrali, N. Taebnia, C. P. Pennisi, F. B. Kadumudi, J. Foroughi, M. Hasany, M. Nikkhah, M. Akbari and G. Orive, *Advanced Science*, 2019, **6**, 1801664.
41. N. Barroso, O. Guaresti, L. Pérez-Álvarez, L. Ruiz-Rubio, N. Gabilondo and J. L. Vilas-Vilela, *European Polymer Journal*, 2019, **120**, 109268.
42. W. Diao, L. Wu, X. Ma, Z. Zhuang, S. Li, X. Bu and Y. Fang, *Journal of Applied Polymer Science*, 2019, **136**, 47783.
43. S. Potiwiput, H. Tan, G. Yuan, S. Li, T. Zhou, J. Li, Y. Jia, D. Xiong, X. Hu and Z. Ling, *Materials Chemistry and Physics*, 2020, **241**, 122354.
44. M. Guvendiren, H. D. Lu and J. A. Burdick, *Soft matter*, 2012, **8**, 260-272.
45. Z. Deng, Y. He, Y. J. Wang, Y. Zhao and L. Chen, *Soft matter*, 2020, **16**, 6128-6137.
46. X. Zhao, Q. Li, X. Ma, F. Quan, J. Wang and Y. Xia, *Journal of Industrial and Engineering Chemistry*, 2015, **24**, 188-195.
47. R. C. Goy, D. d. Britto and O. B. Assis, *Polímeros*, 2009, **19**, 241-247.
48. N. Bhardwaj and S. C. Kundu, *Carbohydrate Polymers*, 2011, **85**, 325-333.
49. A. Rasool, S. Ata and A. Islam, *Carbohydrate polymers*, 2019, **203**, 423-429.
50. T. Kreller, T. Distler, S. Heid, S. Gerth, R. Detsch and A. Boccaccini, *Materials & Design*, 2021, 109877.
51. A. Aljawish, L. Muniglia, A. Klouj, J. Jasniewski, J. Scher and S. Desobry, *Food Hydrocolloids*, 2016, **60**, 551-558.
52. Q. Li, S. Xu, Q. Feng, Q. Dai, L. Yao, Y. Zhang, H. Gao, H. Dong, D. Chen and X. Cao, *Bioactive materials*, 2021, **6**, 3396-3410.
53. T. M. Valentin, A. K. Landauer, L. C. Morales, E. M. DuBois, S. Shukla, M. Liu, L. H. S. Valentin, C. Franck, P.-Y. Chen and I. Y. Wong, *Carbon*, 2019, **143**, 447-456.
54. O. Jeon, Y. B. Lee, T. J. Hinton, A. W. Feinberg and E. Alsberg, *Materials Today Chemistry*, 2019, **12**, 61-70.
55. J. H. Teoh, A. Mozhi, V. Sunil, S. M. Tay, J. Fuh and C. H. Wang, *Advanced Functional Materials*, 2021, 2105932.
56. A. H. Williams, S. Roh, A. R. Jacob, S. D. Stoyanov, L. Hsiao and O. D. Velev, *Nature communications*, 2021, **12**, 1-9.
57. Z. Lin, M. Wu, H. He, Q. Liang, C. Hu, Z. Zeng, D. Cheng, G. Wang, D. Chen and H. Pan, *Advanced Functional Materials*, 2019, **29**, 1808439.
58. M. Gierszewska, J. Ostrowska-Czubenko and E. Chrzanowska, *European Polymer Journal*, 2018, **101**, 282-290.
59. O. Chaudhuri, J. Cooper-White, P. A. Janmey, D. J. Mooney and V. B. Shenoy, *Nature*, 2020, **584**, 535-546.

60. C. Yu, J. Schimelman, P. Wang, K. L. Miller, X. Ma, S. You, J. Guan, B. Sun, W. Zhu and S. Chen, *Chemical reviews*, 2020, **120**, 10695-10743.
61. D. Han, C. Farino, C. Yang, T. Scott, D. Browe, W. Choi, J. W. Freeman and H. Lee, *ACS applied materials & interfaces*, 2018, **10**, 17512-17518.
62. F. Ding, B. Hu, S. Lan and H. Wang, *Food Packaging and Shelf Life*, 2020, **26**, 100559.
63. C. Tonda-Turo, I. Carmagnola, A. Chiappone, Z. Feng, G. Ciardelli, M. Hakkarainen and M. Sangermano, *Bioprinting*, 2020, **18**, e00082.
64. D. Lee, J. P. Park, M.-Y. Koh, P. Kim, J. Lee, M. Shin and H. Lee, *Biomaterials science*, 2018, **6**, 1040-1047.
65. Y. Liu, S. Sakai and M. Taya, *Acta biomaterialia*, 2013, **9**, 6616-6623.
66. D. L. Tran, P. Le Thi, T. T. H. Thi and K. D. Park, *Progress in Natural Science: Materials International*, 2020, **30**, 661-668.
67. G. Tao, R. Cai, Y. Wang, H. Zuo and H. He, *Materials Science and Engineering: C*, 2021, **119**, 111597.
68. Y. Liang, X. Zhao, T. Hu, Y. Han and B. Guo, *Journal of colloid and interface science*, 2019, **556**, 514-528.

Synergistically complexation of phenol functionalized polymer induced in-situ microfiber formation for 3D printing of marine-based hydrogel

[a]Hafez Jafari*, [b]Christine Delporte, [c]Katrien V. Bernaerts, [d]Houman Alimoradi, [e]Lei Nie, [f]Daria Podstawczyk, [g]Kam Chiu Tam*, ' [a]Amin Shavandi*

Materials abbreviation list:

Ch-Ph: chitosan conjugated propionic acid (refer to the gel precursor)

Alg-Ty: Alginate conjugated tyramine (refer to the gel precursor)

PHEC: Phenolated polyelectrolyte complex (mixture of Ch-Ph and Alg-Ty, refer to gel precursor)

PEC: Polyelectrolyte complex

Ch: Chitosan hydrogel using Ch-Ph gel precursor

Alg: Alginate hydrogel using Alg-Ty gel precursor

DCCA: Double crosslinked chitosan-alginate hydrogel using PHEC gel precursor

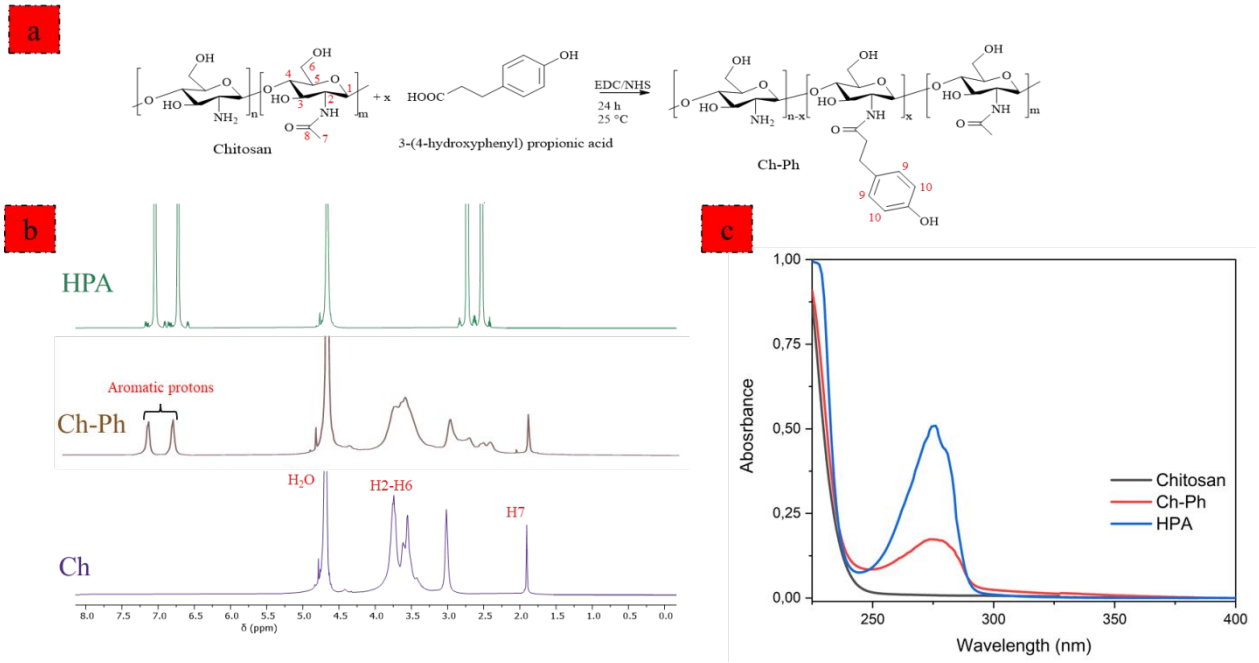

Figure S1. a) Synthetic mechanism of Ch-Ph preparation b) ^{1}H NMR in D_2O and c) UV-vis spectra of the Ch-Ph conjugate, chitosan and HPA,

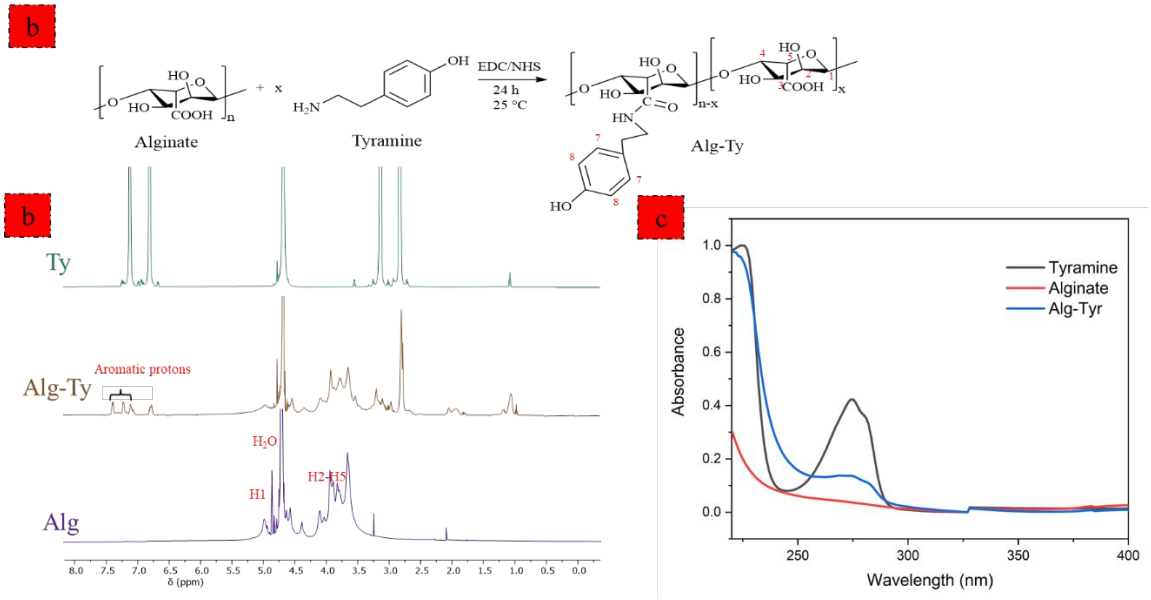

Figure S2. Synthetic scheme of the Alg-Ty, e) ^{1}H NMR in D_2O, and f) UV-Vis spectra of tyramine, Alg-Ty, and alginate.

Table S1. Gelation time of hydrogels based on chitosan, alginate, and their mixture.

Sample name	Concentration (wt%)		Gel time (sec)
	Chitosan-Phenol	Alginate-Tyramine	
$Ch_{0.5}$	0.5	0	52 ± 4
Ch_{1}	1	0	28 ± 3
$Ch_{1.5}$	1.5	0	14 ± 1
$Alg_{0.5}$	0	0.5	422 ± 9
Alg_{1}	0	1	354 ± 5
$Alg_{1.5}$	0	1.5	189 ± 7
$Ch_{0.5}$- $Alg_{0.5}$	0.5	0.5	68 ± 4
$Ch_{0.5}$- Alg_{1}	0.5	1	57 ± 5
$Ch_{0.5}$- $Alg_{1.5}$	0.5	1.5	47 ± 3
Ch_{1}- $Alg_{0.5}$	1	0.5	54 ± 5
Ch_{1}- Alg_{1}	1	1	42 ± 4
Ch_{1}- $Alg_{1.5}$	1	1.5	36 ± 3
$Ch_{1.5}$- $Alg_{0.5}$	1.5	0.5	34 ± 4
$Ch_{1.5}$- Alg_{1}	1.5	1	28 ± 4
$Ch_{1.5}$- $Alg_{1.5}$	1.5	1.5	23 ± 2

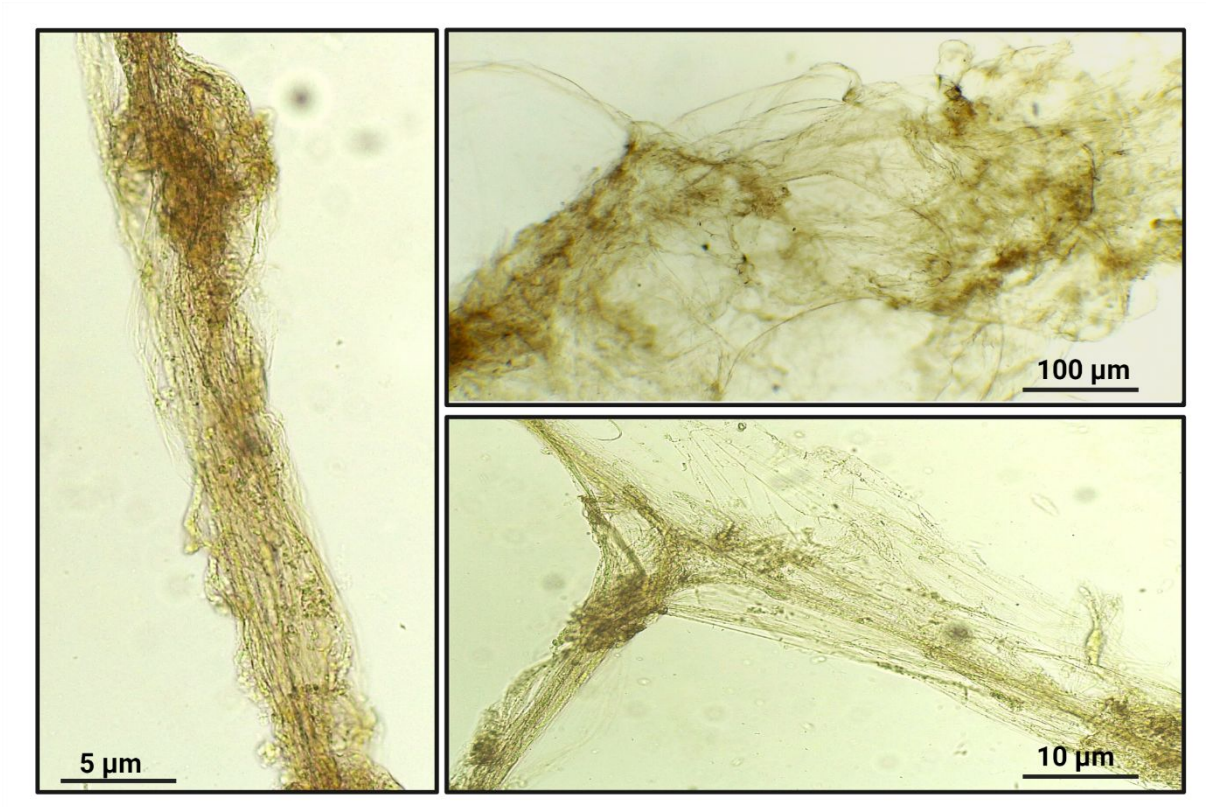

Figure S3. Optical microscopy images of in situ phenol functionalized microfibers

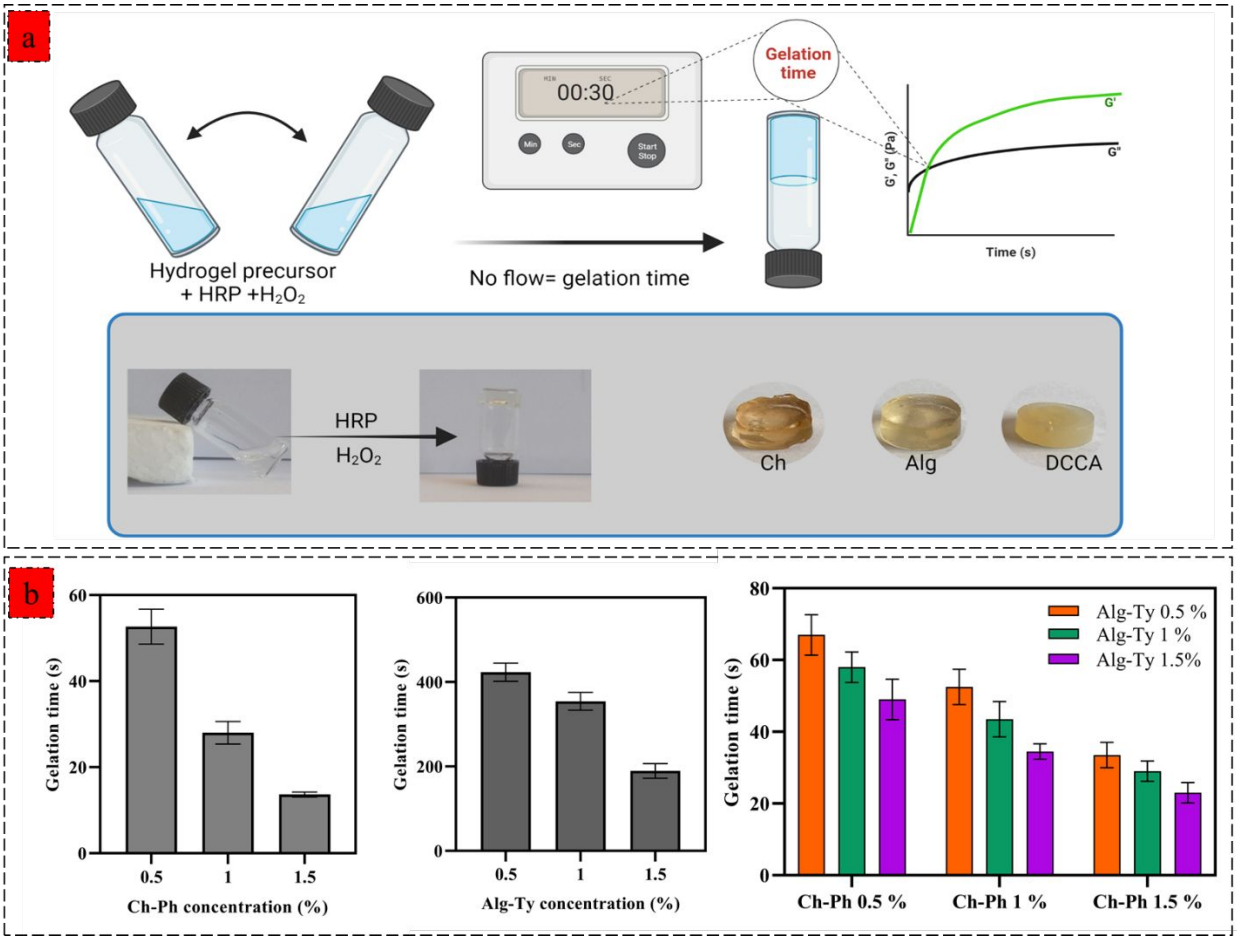

Figure S4. a) Schematic representation of the vial tilting method for gelation time record and photograph of Ch, Alg and DCCA hydrogels. b) Gelation time of Ch hydrogels at different concentrations (0.5, 1, 1.5 wt%) , d) Gelation time of Alg hydrogels at different concentrations (0.5, 1, 1.5 wt%). e) Gelation time of dual crosslinked (DCCA) hydrogels at different concentrations of Ch-Ph (0.5, 1, 1.5 wt%) and Alg-Ty (0.5, 1, 1.5 wt%). Results are expressed as gel time and are the mean ± SD of three independent experiments.

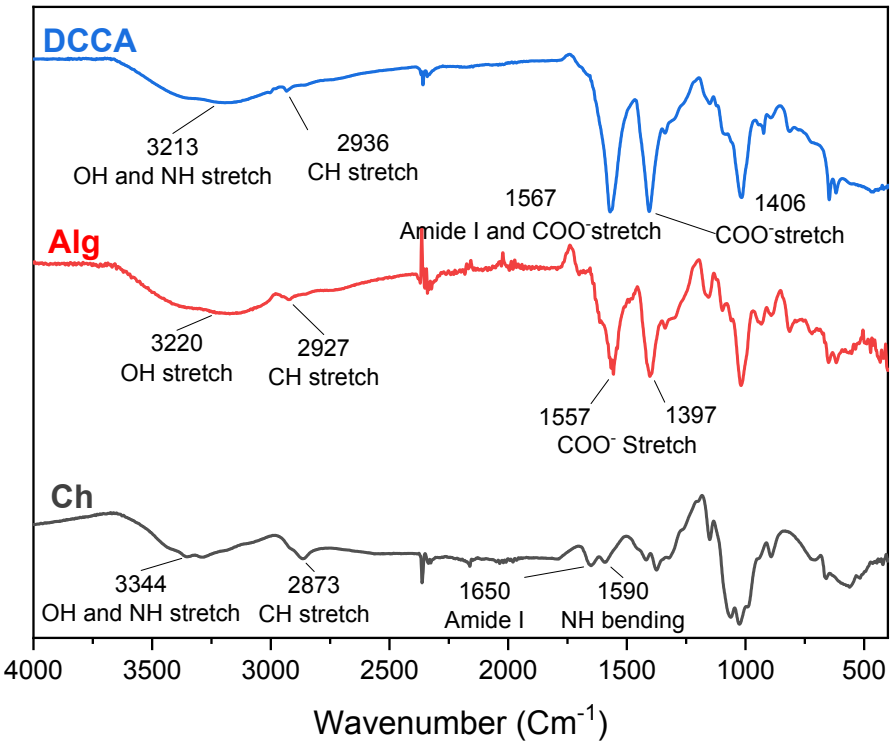

Figure S5. FT-IR spectra of Ch, Alg, and DCCA hydrogel.

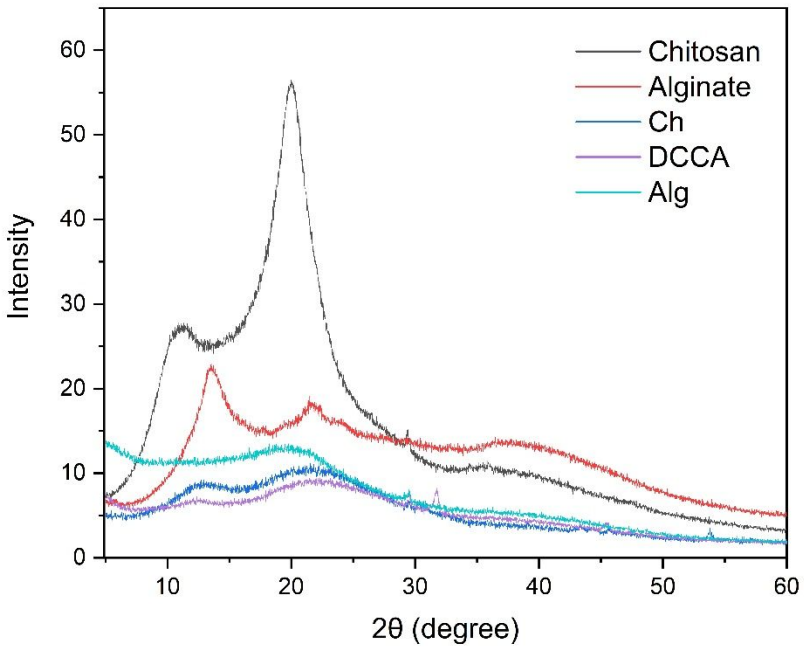

Figure S6. X-ray diffraction analysis of chitosan powder, alginate powder, freeze-dried Ch, Alg, and DCCA hydrogels.

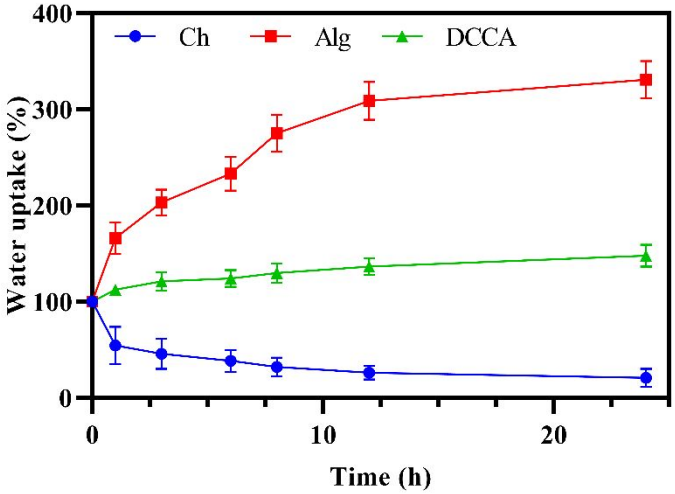

Figure S7. The swelling ratio of Ch, Alg and DCCA hydrogels over a 24h period in PBS at 37 °C

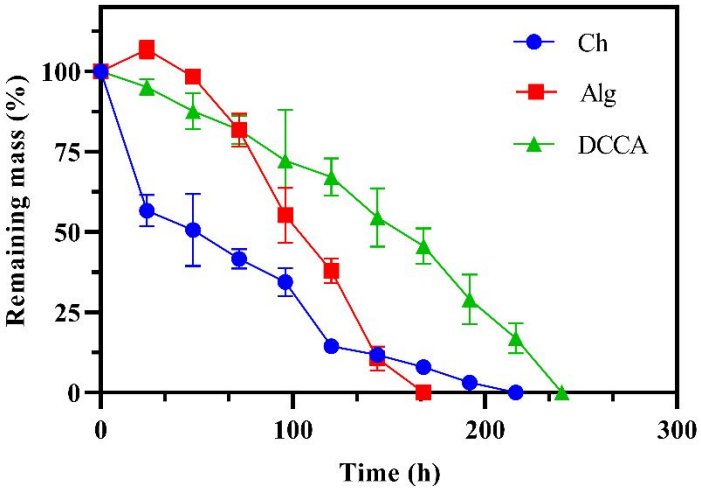

Figure S8. The degradation rate of Ch, Alg and DCCA hydrogels in lysozyme solution (1 mg/mL) at 37 °C.

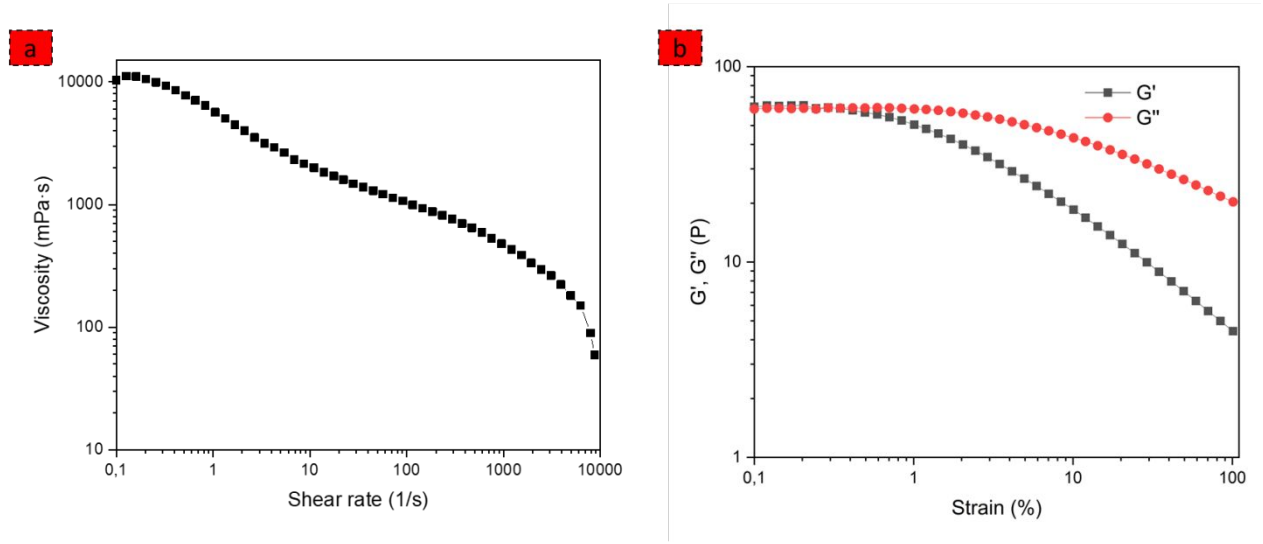

Figure S9. Dynamic viscosity of PHEC ink (2% polymer concentration) over the range of shear rates (0.1-1000 1/s at 37 °C). Storage modulus (G') and loss modulus (G")–strain dependence of Ch, Alg and DCCA ink (2% polymer concentration) at a constant frequency of 1 Hz at 37 °C.

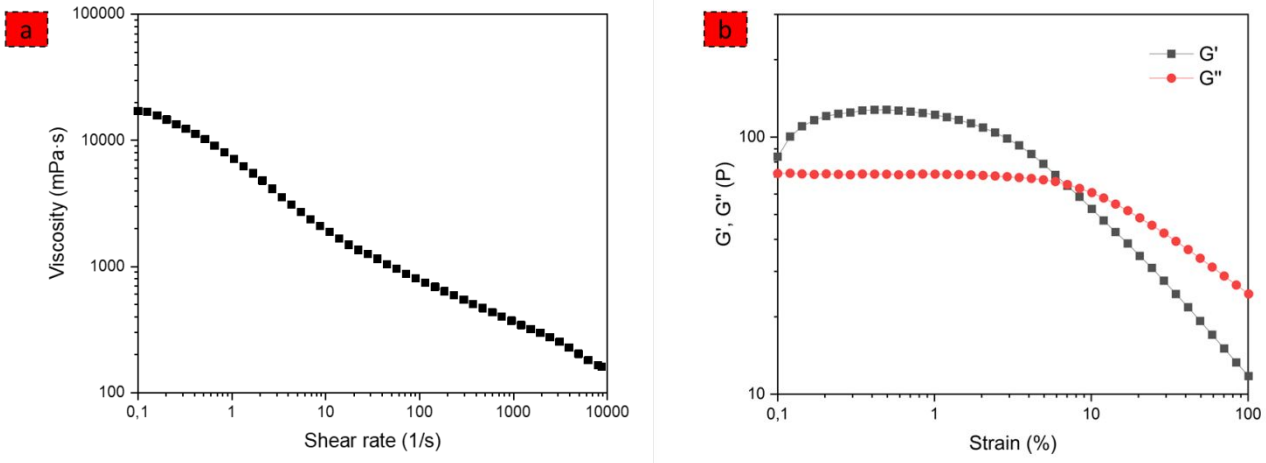

Figure S10. Dynamic viscosity of PHEC ink (2.5 % polymer concentration) over the range of shear rates (0.1-1000 1/s at 37 °C). Storage modulus (G') and loss modulus (G")–strain dependence of Ch, Alg and DCCA ink (2.5 % polymer concentration) at a constant frequency of 1 Hz at 37 °C.

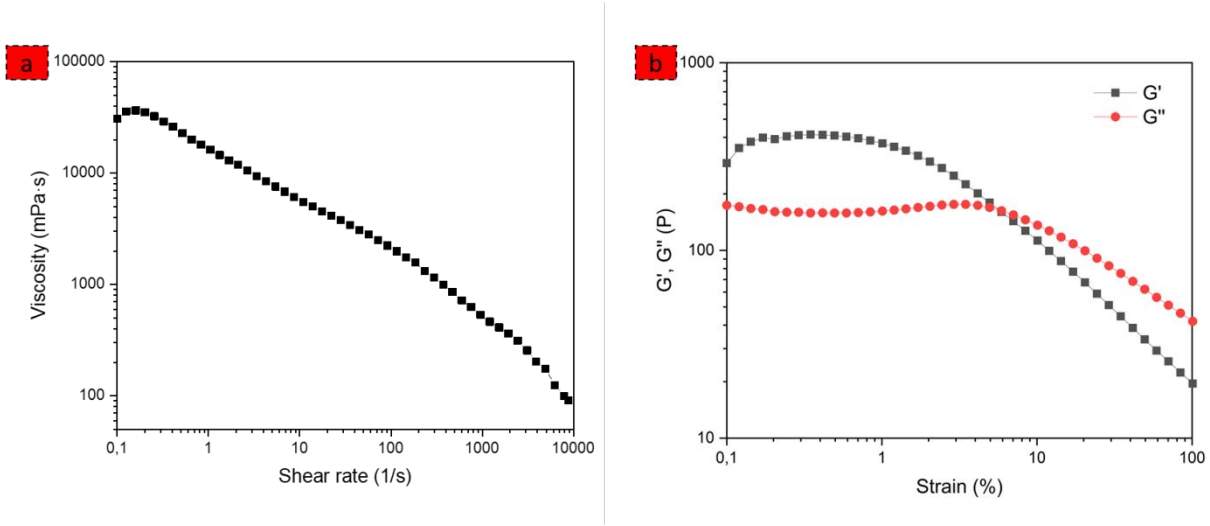

Figure S11. Dynamic viscosity of PHEC ink (3 % polymer concentration) over the range of shear rates (0.1-1000 1/s at 37 °C). Storage modulus (G') and loss modulus (G")–strain dependence of Ch, Alg and DCCA ink (3 % polymer concentration) at a constant frequency of 1 Hz at 37 °C.

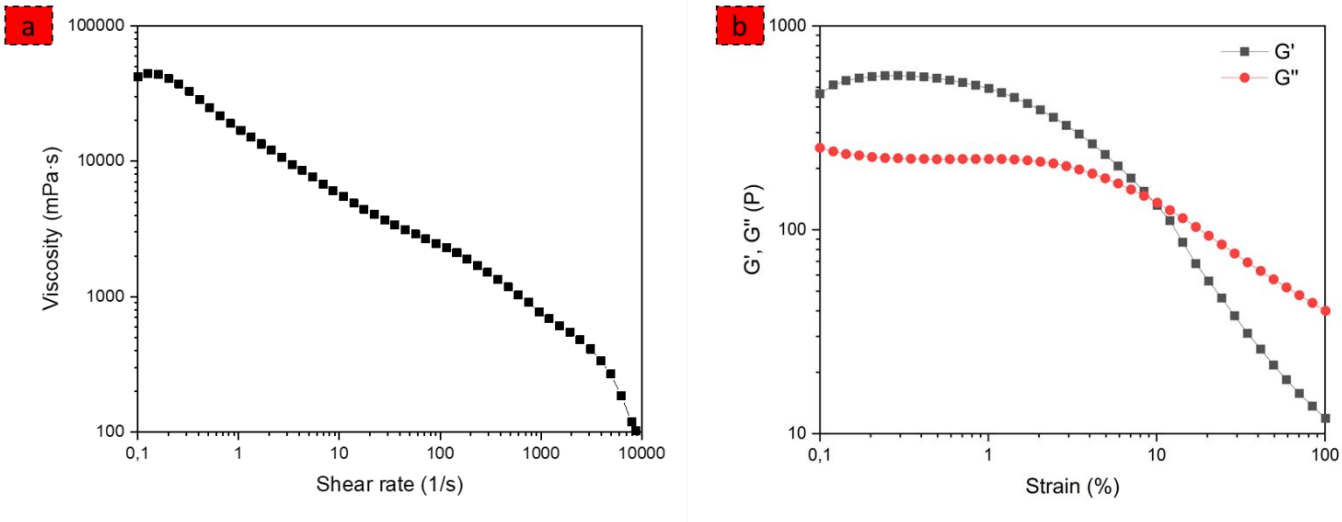

Figure S12. Dynamic viscosity of PHEC ink (3.5 % polymer concentration) over the range of shear rates (0.1-1000 1/s at 37 °C). Storage modulus (G') and loss modulus (G")–strain dependence of Ch, Alg and DCCA ink (3.5 % polymer concentration) at a constant frequency of 1 Hz at 37 °C.

Supplementary Notes 1: **Swelling ratio of hydrogels**

The swelling ratio of hydrogels was evaluated using the method previously described [1]. First, 400 µL of hydrogels was formed and incubated in a PBS solution (pH=7.4) at 37°C. The hydrogels were weighed over time. Briefly, the hydrogels were removed from the solution, and the excess water was removed with filter paper before weighting. The swelling ratio was then determined with the following equation:

$$\text{Swelling ratio } (\%) = \frac{Wt}{Wi}.100\% \quad (1)$$

where W_t and W_i are respectively the wet weight measured at each interval of time and the initial weight.

Supplementary Notes 2: **Degradation rate of hydrogels**

The hydrogel mass change in lysozyme solution was monitored as described in previous studies [2]. Briefly, 400 µL hydrogels were weighted (W_i) and then immersed in a PBS solution containing 1mg/mL of lysozyme (pH 7.4) and incubated at 37°C. The lysozyme solution was renewed every three days during the experiment. At a certain time-point, the hydrogels were removed from the solution and weighed (W_t). The remaining weight ratio is calculated using equation (2).

$$\text{Remaining weight } (\%) = \frac{Wt}{Wi}.100\% \quad (2)$$

Supplementary Notes 3: **Antioxidant activity**

DPPH[1] radical scavenging assay was performed to investigate the antioxidant activity of hydrogels according to a previously reported method [3]. 300µL of hydrogels were prepared in a 48-well plate. Then, 1 mL of ethanol containing 100µL of DDPH solution (0.5 mM) was added and incubated for 60 min in the dark. 300µL of deionized water (DIW) was used for the control group. The absorbance at 517 nm of the reaction mixture was measured, and the scavenging effect of hydrogels on DPPH radicals was calculated using equation (3).

$$\text{Radical scavenging activity } (\%) = [1 - (As/Ac)] \times 100 \quad (3)$$

Where A_s and A_C are the absorbances of samples, and the control (DIW), respectively.

Supplementary Notes 4: **Antibacterial activity**

The antibacterial activity of the hydrogels against gram-negative bacteria (*E.Coli*) and gram-positive bacteria (*S.aureus*) were investigated using the growth inhibition assay [4] and disk diffusion test [5]. Briefly, 100 µL/well hydrogels were formed in a 48 wells plate, and 1 mL of bacterial suspension (10^5 CFU/mL) inoculated into Muller–Hinton (M–H) was added to the wells and incubated for 24 h at 37 °C. 200 µL of bacterial suspensions were transferred to 96-well plates, and the absorbance was measured using a microplate reader (Epoch plate reader, BioTek®, USA).

For the disk diffusion test, 100µL of the bacterial suspension (10^6 CFU/mL) was uniformly spread on an agar plate. The hydrogels prepared in cylindrical shape were deposited on the top of the agar plate and incubated for 24 h at 37 °C. The inhibition zone around each sample was recorded as the antibacterial effect of the hydrogels

Supplementary Notes 5: **3D cell encapsulation**

For 3D cell encapsulation, sterile gel precursors and a 3T3-L1 cell suspension were mixed with HRP to obtain a homogenous solution with a final cell density of 5×10^5 cells/mL. Then, 50 µL of cell encapsulated gel precursors containing HRP were mixed with 50 µL gel precursors containing H_2O_2

[1] 2,2-diphenyl-1-picryl-hydrazyl-hydrate

(1mM) in a Millicell EZ SLIDE 8-well glass (Merck, Kenilworth, NJ, USA) and the hydrogels were incubated at 37 °C for 30 min to form a stable hydrogel. The cell encapsulated hydrogels were cultured with 1 mL DMEM (Dulbecco's Modified Eagle Medium) supplemented with 10 % fetal calf serum (FCS), 200U/mL penicillin and 200U/mL streptomycin. The hydrogels were incubated at 37 °C for 1 or 3 days, and cell viability at days 1, and 3 was determined using Hoechst/ethidium homodimer I (EH1) staining. Briefly, cell nuclei were stained using 10 μM Hoechst (H33342 Sigma, MA, USA) and EH1 (E1903 Sigma MA, USA) and incubated for 20 min. Then, the cells were washed two times with PBS. The cell nuclei distribution and morphology were analyzed using a fluorescent microscope (Zoe fluorescent cell imager, Biorad, Hercules, CA).

References

1. E. Jooybar, M. J. Abdekhodaie, M. Alvi, A. Mousavi, M. Karperien and P. J. Dijkstra, *Acta biomaterialia*, 2019, **83**, 233-244.
2. H. Jafari, A. Dadashzadeh, S. Moghassemi, P. Zahedi, C. A. Amorim and A. Shavandi, *Gels*, 2021, **7**, 138.
3. D. L. Tran, P. Le Thi, T. T. H. Thi and K. D. Park, *Progress in Natural Science: Materials International*, 2020, **30**, 661-668.
4. G. Tao, R. Cai, Y. Wang, H. Zuo and H. He, *Materials Science and Engineering: C*, 2021, **119**, 111597.
5. Y. Liang, X. Zhao, T. Hu, Y. Han and B. Guo, *Journal of colloid and interface science*, 2019, **556**, 514-528.